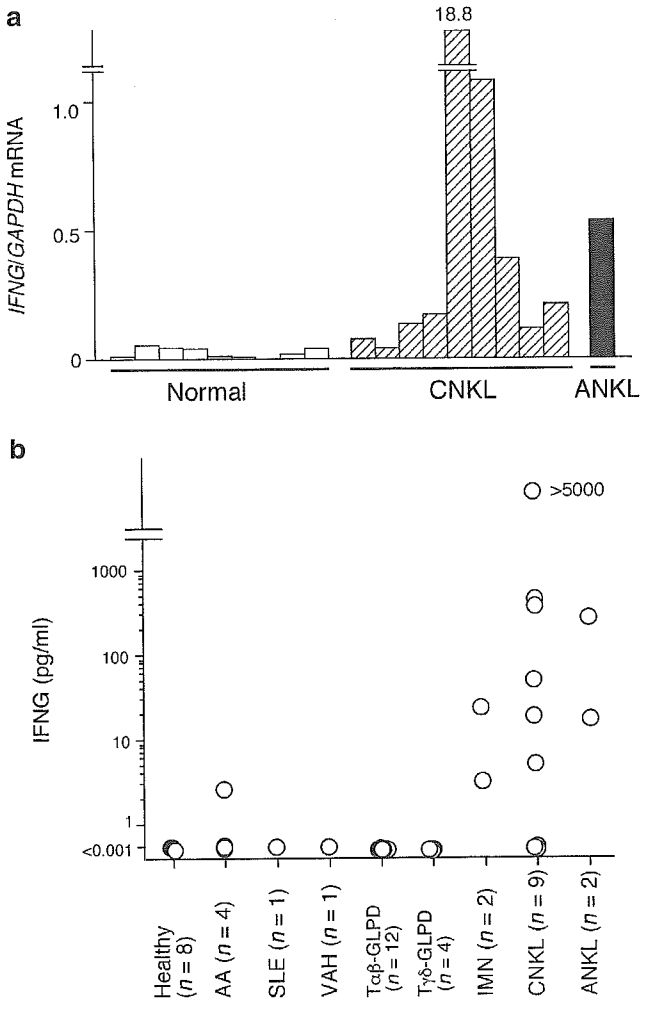

Figure 6 Confirmation of overexpression of IFNG. (a) Quantitation of *IFNG* mRNA in NK cell fractions. Complementary DNA was prepared from the NK cell fractions, and was subjected to real-time RT-PCR analysis with primers specific for the *IFNG* or *GAPDH* genes. The ratio of the abundance of *IFNG* mRNA to that of *GAPDH* mRNA was calculated as 2^n, where n is the C_T value for *GAPDH* cDNA minus the C_T value for *IFNG* cDNA. (b) Sera were obtained from healthy volunteers (healthy) and individuals with aplastic anemia (AA), systemic lupus erythematosus (SLE), virus infection-associated hemophagocytic syndrome (VAH), LDGL of $\alpha\beta^+$ T cell, LDGL of $\gamma\delta^+$ T cell, infectious mononucleosis (IMN), CNKL, or ANKL. The expression level of IFNG protein in the sera was determined by flow cytometry, and shown as pg/ml.

intrinsic for an accurate comparison of the disease status, since simple comparison with PB MNCs would be severely influenced by any changes in the cell composition of PB MNCs in each individual.

However, even by using expression profiles of the purified fractions, similarity of the expression pattern of all gene set failed to clearly separate the affected NK cells from normal ones (Figure 2b), indicating the necessity of a diagnostic system with a 'supervised' algorithm. For this aim, we first extracted gene clusters, expression of which was specific to either normal or affected NK cells. Correspondence analysis on the expression patterns of such 'LDGL-associated genes' has succeeded in the reduction of the number of pattern dimensions into three. To our surprise, projection of all samples into this 3D space clearly demonstrated that the affected NK cells (CNKL/ANKL) were placed clustered at a position separate from that of normal NK cells (Figure 3c). With coordinates in such decomposited dimensions, we then invented a novel class prediction means, 'weighted-distance method'. As expected from the clear separation in the 3D view, the weighted-distance method provided correct prediction for all samples studied. A cross-validation trial for the disease diagnosis also gave a highly accurate prediction rate (77.8%).

Given a high incidence of clonal EBV infection in ANKL cells, EBV is believed to play an essential role in the pathogenesis of this fulminant disorder. From the point of view of gene-expression profile, the NK cells positive for EBV infection (CNKL-9 and ANKL-1) shared gene-expression patterns characteristic to other indolent CNKL cells. For instance, a comparison of normal NK cells and CNKL samples (except EBV^+ CNKL-9) has identified a total of nine CNKL-related genes including those for nuclear matrix protein-2 (GenBank accession number, D50926), cytochrome *C* (D00265), tyrosine 3-monooxygenase/tryptophan 5-monooxygenase activation protein, theta polypeptide or 14-3-3 protein tau (X56468), O-linked GlcNAc transferase (AL050366), IFNG, chemokine C–C motif receptor 1 (CCR1; D10925), chondroitin sulfate proteoglycan 2 (X15998), and fibrinogen-like 2 (AI432401). The 3D view of the correspondence analysis for these 'CNKL-associated' genes clearly demonstrated that the EBV^+ CNKL-9 subject was included in the other indolent CNKL group (Figure 4a). Similarly, another EBV^+ subject (ANKL-1) was placed closely with the CNKL samples, according to the expression profiles of the genes which differentiated CNKL cells from normal NK cells (Figure 4b).

These data propose a hypothesis that gene-expression alterations characteristic to an activated, yet indolent, proliferation of NK cells found in CNKL patients also take place in the highly proliferating NK cells in EBV^+ individuals. In other words, a similar mechanism may be utilized for the sustained outgrowth of NK cells both in the individuals with CNKL and ANKL. It should be emphasized, however, that the number of EBV^+ samples ($n=2$) in these analyses was too small to extract any conclusive remarks on the pathophysiology of proliferating EBV^+ NK cells. Nevertheless, we believe that it was interesting to find that EBV^+ NK cells may share a molecular signature with EBV^- LDGL cells.

We finally tried to identify single-gene markers, the presence or absence of which helps the diagnosis of LDGL. A total of 22 genes were shown to be specific to normal NK cells, including those for cyclin-dependent kinase inhibitor 1A (CDKN1A; GenBank accession number U03106) or CIP1, dual-specificity phosphatase 6 (DUSP6; AB013382), toll-like receptor 2 (TLR2; AF051152), tissue inhibitor of metalloproteinase 1 (TIMP1; D11139), and aldo-keto reductase family 1 member C3 (AKR1C3; D17793) (Figure 5b).

CDKN1A is transcriptionally regulated by the activity of p53, and functions as a major effector for antitumor activity of p53, through the suppression of cyclin-dependent kinase activities.[32] Therefore, loss of expression of *CDKN1A* may allow uncontrolled transition at the G_2–M boundary in the cell cycle, and may partially account for the overgrowth of NK cells in LDGL individuals. Similarly, DUSP6 antagonizes MAPK activities *via* dephosphorylation of the latter kinases.[33] Decrease of DUSP6 expression may therefore contribute to overactivation of MAPK and to enhanced mitogenesis.

AKR1C3 catalyzes conversion of aldehydes and ketones to alcohols *in vivo*. Although its role in NK cells is unknown yet, downregulation of its transcription has been also reported in the

LGLs of T cell-type LDGL.[19] Comparison with DNA microarray of $CD4^{-}CD8^{+}$ T-cells between healthy individuals and those with T cell-type LDGL has identified the *AKR1C3* gene as the specific marker to the former. Decrease of *AKR1C3* message was also confirmed by quantitative 'real-time' RT-PCR method in those patients. Transcriptional suppression of *AKR1C3* was thus revealed in affected LGLs for both NK cell- and T cell-type LDGL, and may be a common marker for the diagnosis of LDGL condition.

A number of growth-promoting factors were found in the 'LDGL-specific genes' in Figure 5a. IFNG and BIRC3[34] are, for instance, known to protect NK cells from apoptosis, and IRF4 has an oncogenic activity *in vivo*.[35] Additionally, CHD1 contains an SNF2-related helicase/ATPase domain, and is presumed to be involved in the regulation of chromatin structure and gene transcription as well.[36]

Our data, together with that by Mizuno *et al*[31] suggest that the serum concentration of IFNG protein may be an indicator of NK cell-type LDGL. Direct production of IFNG by affected NK cells may also imply the presence of an autocrine loop for the NK cell growth.

The mechanism by which affected NK cells produce IFNG is still to be revealed. It is known that IL-2, IL-12, IL-15, and IL-18 all activate production of IFNG in NK cells. In our microarray data set, however, none of IL-2, IL-12, and IL-18 were found to be significantly expressed in the subjects (not shown). Although IL-15 was moderately expressed in our NK samples, its expression level did not differ between normal and affected NK cells. In support of this notion, we could not detect significant level of IL-2 protein in the examination of serum level of cytokines (not shown). Therefore, it is currently an open question as to whether activation of *IFNG* transcription in the affected NK cells is a secondary event from the stimulation by other cells such as T cells, or intracellular mechanism of IFNG expression is deregulated in the affected NK cells.

Conclusion

We have characterized the transcriptome of a relatively uncommon disorder, NK cell-type LDGL. Comparison of purified NK cells between healthy and CNKL individuals led to the identification of gene sets which are useful in the expression profile-based differential diagnosis of the disorder. Such disease-associated genes have also provided us insights into the molecular pathogenesis of NK cell-type LDGL. Together with further optimization of statistical methods, increase in the number of both genes and subjects for the analysis would help to define and clarify the clinical entities of NK cell disorders.

Acknowledgements

We thank all patients, healthy volunteers, and physicians who participated in the collection of NK cell depository. We are also grateful to Dr T Miwa for his helpful suggestions.

Supplementary Information

Supplementary Information accompanies the paper on the Leukemia website (http://www.nature.com/leu).

References

1 Loughran Jr TP. Clonal diseases of large granular lymphocytes. *Blood* 1993; **82**: 1–14.
2 Semenzato G, Zambello R, Starkebaum G, Oshimi K, Loughran Jr TP. The lymphoproliferative disease of granular lymphocytes: updated criteria for diagnosis. *Blood* 1997; **89**: 256–260.
3 Oshimi K. Granular lymphocyte proliferative disorders: report of 12 cases and review of the literature. *Leukemia* 1988; **2**: 617–627.
4 Loughran Jr TP, Starkebaum G. Large granular lymphocyte leukemia. Report of 38 cases and review of the literature. *Medicine (Baltimore)* 1987; **66**: 397–405.
5 Jaffe ES, Harris NL, Stein H, Vardiman JW (eds). *Pathology and Genetics of Tumours of Haematopoietic and Lymphoid Tissues*. Lyon: IARC Press, 2001.
6 Gelb AB, van de Rijn M, Regula Jr DP, Cornbleet JP, Kamel OW, Horoupian DS *et al*. Epstein–Barr virus-associated natural killer-large granular lymphocyte leukemia. *Hum Pathol* 1994; **25**: 953–960.
7 Tefferi A. Chronic natural killer cell lymphocytosis. *Leuk Lymphoma* 1996; **20**: 245–248.
8 Rabbani GR, Phyliky RL, Tefferi A. A long-term study of patients with chronic natural killer cell lymphocytosis. *Br J Haematol* 1999; **106**: 960–966.
9 Nash R, McSweeney P, Zambello R, Semenzato G, Loughran Jr TP. Clonal studies of CD3-lymphoproliferative disease of granular lymphocytes. *Blood* 1993; **81**: 2363–2368.
10 Garcia-Suarez J, Prieto A, Reyes E, Arribalzaga K, Perez-Machado MA, Lopez-Rubio M *et al*. Persistent lymphocytosis of natural killer cells in autoimmune thrombocytopenic purpura (ATP) patients after splenectomy. *Br J Haematol* 1995; **89**: 653–655.
11 Ohno Y, Amakawa R, Fukuhara S, Huang CR, Kamesaki H, Amano H *et al*. Acute transformation of chronic large granular lymphocyte leukemia associated with additional chromosome abnormality. *Cancer* 1989; **64**: 63–67.
12 Tefferi A, Greipp PR, Leibson PJ, Thibodeau SN. Demonstration of clonality, by X-linked DNA analysis, in chronic natural killer cell lymphocytosis and successful therapy with oral cyclophosphamide. *Leukemia* 1992; **6**: 477–480.
13 Morice WG, Kurtin PJ, Leibson PJ, Tefferi A, Hanson CA. Demonstration of aberrant T-cell and natural killer-cell antigen expression in all cases of granular lymphocytic leukaemia. *Br J Haematol* 2003; **120**: 1026–1036.
14 Cheung VG, Morley M, Aguilar F, Massimi A, Kucherlapati R, Childs G. Making and reading microarrays. *Nat Genet* 1999; **21**: 15–19.
15 Duggan DJ, Bittner M, Chen Y, Meltzer P, Trent JM. Expression profiling using cDNA microarrays. *Nat Genet* 1999; **21**: 10–14.
16 Dhanasekaran SM, Barrette TR, Ghosh D, Shah R, Varambally S, Kurachi K *et al*. Delineation of prognostic biomarkers in prostate cancer. *Nature* 2001; **412**: 822–826.
17 Miyazato A, Ueno S, Ohmine K, Ueda M, Yoshida K, Yamashita Y *et al*. Identification of myelodysplastic syndrome-specific genes by DNA microarray analysis with purified hematopoietic stem cell fraction. *Blood* 2001; **98**: 422–427.
18 Ohmine K, Ota J, Ueda M, Ueno S-i, Yoshida K, Yamashita Y *et al*. Characterization of stage progression in chronic myeloid leukemia by DNA microarray with purified hematopoietic stem cells. *Oncogene* 2001; **20**: 8249–8257.
19 Makishima H, Ishida F, Ito T, Kitano K, Ueno S, Ohmine K *et al*. DNA microarray analysis of T cell-type lymphoproliferative disease of granular lymphocytes. *Br J Haematol* 2002; **118**: 462–469.
20 Van Gelder RN, von Zastrow ME, Yool A, Dement WC, Barchas JD, Eberwine JH. Amplified RNA synthesized from limited quantities of heterogeneous cDNA. *Proc Natl Acad Sci USA* 1990; **87**: 1663–1667.
21 Fellenberg K, Hauser NC, Brors B, Neutzner A, Hoheisel JD, Vingron M. Correspondence analysis applied to microarray data. *Proc Natl Acad Sci USA* 2001; **98**: 10781–10786.
22 Alon U, Barkai N, Notterman DA, Gish K, Ybarra S, Mack D *et al*. Broad patterns of gene expression revealed by clustering analysis of tumor and normal colon tissues probed by oligonucleotide arrays. *Proc Natl Acad Sci USA* 1999; **96**: 6745–6750.

23 Ramaswamy S, Ross KN, Lander ES, Golub TR. A molecular signature of metastasis in primary solid tumors. *Nat Genet* 2003; **33**: 49–54.
24 Alkema MJ, Wiegant J, Raap AK, Berns A, van Lohuizen M. Characterization and chromosomal localization of the human proto-oncogene BMI-1. *Hum Mol Genet* 1993; **2**: 1597–1603.
25 Park IK, Qian D, Kiel M, Becker MW, Pihalja M, Weissman IL *et al.* Bmi-1 is required for maintenance of adult self-renewing haematopoietic stem cells. *Nature* 2003; **423**: 302–305.
26 Lessard J, Sauvageau G. Bmi-1 determines the proliferative capacity of normal and leukaemic stem cells. *Nature* 2003; **423**: 255–260.
27 Meagher MJ, Braun RE. Requirement for the murine zinc finger protein ZFR in perigastrulation growth and survival. *Mol Cell Biol* 2001; **21**: 2880–2890.
28 Thornton S, Kuhn KA, Finkelman FD, Hirsch R. NK cells secrete high levels of IFN-gamma in response to in vivo administration of IL-2. *Eur J Immunol* 2001; **31**: 3355–3360.
29 Ross ME, Caligiuri MA. Cytokine-induced apoptosis of human natural killer cells identifies a novel mechanism to regulate the innate immune response. *Blood* 1997; **89**: 910–918.
30 Carson WE, Giri JG, Lindemann MJ, Linett ML, Ahdieh M, Paxton R *et al.* Interleukin (IL) 15 is a novel cytokine that activates human natural killer cells via components of the IL-2 receptor. *J Exp Med* 1994; **180**: 1395–1403.
31 Mizuno S, Akashi K, Ohshima K, Iwasaki H, Miyamoto T, Uchida N *et al.* Interferon-gamma prevents apoptosis in Epstein–Barr virus-infected natural killer cell leukemia in an autocrine fashion. *Blood* 1999; **93**: 3494–3504.
32 El-Deiry WS, Tokino T, Velculescu VE, Levy DB, Parsons R, Trent JM *et al.* WAF1, a potential mediator of p53 tumor suppression. *Cell* 1993; **75**: 817–825.
33 Muda M, Boschert U, Dickinson R, Martinou JC, Martinou I, Camps M *et al.* MKP-3, a novel cytosolic protein-tyrosine phosphatase that exemplifies a new class of mitogen-activated protein kinase phosphatase. *J Biol Chem* 1996; **271**: 4319–4326.
34 Liston P, Roy N, Tamai K, Lefebvre C, Baird S, Cherton-Horvat G *et al.* Suppression of apoptosis in mammalian cells by NAIP and a related family of IAP genes. *Nature* 1996; **379**: 349–353.
35 Iida S, Rao PH, Butler M, Corradini P, Boccadoro M, Klein B *et al.* Deregulation of MUM1/IRF4 by chromosomal translocation in multiple myeloma. *Nat Genet* 1997; **17**: 226–230.
36 Woodage T, Basrai MA, Baxevanis AD, Hieter P, Collins FS. Characterization of the CHD family of proteins. *Proc Natl Acad Sci USA* 1997; **94**: 11472–11477.

Int. J. Cancer: **108,** 237–242 (2004)

Publication of the International Union Against Cancer

MUTATIONS OF *BRAF* ARE ASSOCIATED WITH EXTENSIVE *hMLH1* PROMOTER METHYLATION IN SPORADIC COLORECTAL CARCINOMAS

Koji KOINUMA[1,2], Kazuhisa SHITOH[1], Yasuyuki MIYAKURA[1], Taiji FURUKAWA[1], Yoshihiro YAMASHITA[2], Jun OTA[2], Ruri OHKI[2], Young Lim CHOI[2], Tomoaki WADA[2], Fumio KONISHI[3], Hideo NAGAI[1] and Hiroyuki MANO[2,4]*

[1]*Department of Surgery, Jichi Medical School, Tochigi, Japan*
[2]*Division of Functional Genomics, Jichi Medical School, Tochigi, Japan*
[3]*Department of Surgery, Omiya Medical Center, Jichi Medical School, Saitama, Japan*
[4]*Crest, Japan Science and Technology Agency, Saitama, Japan*

Activating mutations of *BRAF* have been frequently observed in microsatellite unstable (MSI$^+$) colorectal carcinomas (CRCs), in which mutations of *BRAF* and *KRAS* are mutually exclusive. Previously, we reported that hypermethylation of *hMLH1* might play an important role in the tumorigenesis of right-sided sporadic CRCs with MSI showing less frequency of *KRAS/TP53* alteration. Therefore, we have assumed that *BRAF* mutations might be highly associated with *hMLH1* methylation status rather than MSI status. In this study, mutations of *BRAF* and *KRAS* and their relationship with MSI and *hMLH1* methylation status were examined in 140 resected specimens of CRC. The methylation status was classified into 3 types: full methylation (FM), partial methylation (PM) and nonmethylation (NM). Only FM closely linked to reduced expression of hMLH1 protein. *BRAF* mutations were found in 16 cases (11%), all leading to the production of BRAF^{V599E}. As for MSI status, *BRAF* mutations were found in 43% of MSI$^+$ and 4% of MSI$^-$ cases ($p < 0.0001$). Among the MSI$^+$ individuals, *BRAF* mutations were more frequent in cases with hMLH1 deficiency (58%) than those with hMSH2 deficiency (0%; $p = 0.02$). Moreover, they were found in 69% of FM, 4% of PM and 4% of NM, revealing a striking difference between FM and the other 2 groups (FM *vs.* PM or NM; $p < 0.0001$). These findings suggest that BRAF activation may participate in the carcinogenesis of sporadic CRCs with *hMLH1* hypermethylation in the proximal colon, independently of KRAS activation.

Key words: *sporadic colorectal cancer;* BRAF *mutation;* hMLH1 *hypermethylation; microsatellite instability*

In the development of colorectal cancer (CRC), it is now widely accepted that some forms of genetic instability lead to the sequential accumulation of genetic alterations and consequently develop carcinomas.[1] RAS activation in the MAP kinase cascade is supposed to constitute a part of the primary events in colorectal carcinogenesis, and the *KRAS* gene mutations have been found in about 30–40% cases of sporadic CRCs.[2–4]

Recently, activating *BRAF* mutations have been found almost invariably in melanoma cells and sometimes in other types of carcinoma, including CRCs,[5–7] implying a function of *BRAF* as a protooncogene. The *RAF* genes are members of MAPK pathway, encoding serine/threonine kinases that integrate the upstream input signals.[8,9] Once recruited at the cell membrane by GTP-loaded RAS, RAF becomes activated and subsequently phosphorylates the downstream kinases, MEKs, which eventually induce transcriptional activation of the target genes.[9]

More recently, frequent *BRAF* mutations and infrequent *KRAS* mutations have been reported in DNA-mismatch repair (MMR)-deficient CRCs.[10] Inactivation of MMR genes incurs instability of genomic microsatellite sequence (microsatellite instability, or MSI), which is found in the majority of patients with hereditary nonpolyposis colorectal cancer syndrome (HNPCC) and in 10–15% of cases of sporadic CRCs.[11–13] Moreover, it was also reported that 70–90% of sporadic CRCs with MSI (MSI$^+$ CRCs) are associated with hypermethylation of *hMLH1*, one of DNA-MMR genes, and have distinct clinical and pathologic characteristics, *i.e.*, occurrence in older females, location in the proximal colon and histopathology of mucious or poor differentiation.[14–20]

We have previously examined the methylation status of *hMLH1* gene in sporadic CRCs by use of 5 sets of primer spanning the whole CpG sites within its promoter region and have classified the methylation status into 3 subtypes: full methylation, partial methylation and nonmethylation.[21,22] We reported that an extensive methylation, or full methylation, of *hMLH1* promoter was found in about 80% of MSI$^+$ CRC cases and was highly associated with loss of expression of its gene product. Interestingly, this type of CRC cells are rarely associated with *KRAS* mutations and loss of heterozygosity (LOH) of *TP53* gene.[22] It is therefore possible that extensive methylation of *hMLH1* promoter region may contribute to the carcinogenesis of the right-sided sporadic CRCs, independently of *KRAS/p53* alterations.

From these results, 2 questions may arise. First, does the activation of BRAF, instead of KRAS, take part in the carcinogenesis of CRCs with extensive *hMLH1* methylation? Second, if so, does the BRAF activation have any relationship with the CRCs with partial methylation, although most of which are microsatellite stable (MSI$^-$), maintain MMR gene expression and show a relatively high incidence of KRAS and p53 alterations?[22]

Additionally, in the melanoma cells, high frequency of mutations of *β-catenin* and *BRAF* has been recognized.[23] Some researchers previously reported that *β-catenin* mutations were more common in MSI$^+$ CRCs than in MSI$^-$ ones.[19,23–25] However, it has not been elucidated yet whether there are any relationship between the mutations of *β-catenin* and *BRAF* in the CRCs with *hMLH1* hypermethylation.

In this study, we have investigated the frequency of *BRAF* mutation and its relationship with *KRAS* and *β-catenin* mutations in a large consecutive series of sporadic CRCs in regard to both MSI status and degrees of *hMLH1* methylation.

Abbreviations: CRC, colorectal cancer; FM, full methylation; HNPCC, hereditary nonpolyposis colorectal cancer syndrome; LOH, loss of heterozygosity; MAPK, mitogen-activated protein kinase; MAPKKK, mitogen-activated protein kinase kinase kinases; MEK, mitogen-activated protein/extracellular signal-regulated kinase kinase; MGMT, O^6-methylguanine DNA methyltransferase; MMR, mismatch repair; MSI, microsatellite instability; NM, nonmethylation; PM, partial methylation.

*Correspondence to: Division of Functional Genomics, Jichi Medical School, 3311-1 Yakushiji, Minamikawachi-machi, Kawachi-gun, Tochigi 329-0498, Japan. Fax: +81-285-44-7322. E-mail: hmano@jichi.ac.jp

Received 23 May 2003; Revised 4 August 2003; Accepted 25 August 2003

DOI 10.1002/ijc.11523
Published online 27 October 2003 in Wiley InterScience (www.interscience.wiley.com).

MATERIAL AND METHODS

Tumor samples

Tumor samples were obtained from 140 sporadic CRC patients who underwent surgical treatment at the Jichi Medical School Hospital. None of the patients had first-degree relatives with CRC. Informed consents were obtained from all patients, and the ethics committee of the Jichi Medical School approved this study (#02-01). We selected these cases from approximately 380 consecutive series of CRCs previously analyzed for MSI status.[21,26] All the MSI^+ cases were reconfirmed for the MSI status by pentaplex PCR method, whereas MSI^- CRCs were selected so that the gender and tumor site were balanced between the MSI^+ and MSI^- groups (MSI^+, $n = 28$; MSI^-, $n = 112$). The patients were 69 men and 71 women, and their age ranged from 19 to 86 years with a mean of 63 years.

DNA extraction

Genomic DNA was extracted from fresh-frozen samples of tumor by use of QIAamp DNA Mini Kit (Qiagen, Chatsworth, CA) according to the manufacturer's protocol.

BRAF *mutation analysis*

BRAF mutations were analyzed in exons 11 and 15. These exons were chosen because all reported *BRAF* mutations occurred at these regions. PCR was performed with 2–5 ng of genomic DNA as a template by using the same PCR primer as reported previously.[5] PCR condition was as follows: 94°C for 9 min, followed by 35 cycles of 94°C for 1 min, 60°C for 1 min and 72°C for 2 min. The PCR products were purified using a QIAquick spin purification kit (Qiagen), and the purified PCR products were sequenced with BigDye Terminator Cycle Sequencing Ready Reaction kits (PE Applied Biosystems, Foster City, CA), all according to the manufacturers' instructions. Sequencing was performed in both directions using forward and reverse PCR primers. The purified products were run on an ABI 310 PRISM Genetic Analyzer (PE Applied Biosystems). The data were collected and analyzed using the Applied Biosystems sequencing analysis software.

MSI status analysis

MSI was analyzed by using 9 microsatellite repeat loci (3 markers were dinucleotide repeats and 6 were mononucleotide repeats) as described previously.[21] MSI status was stratified as follows according to the criteria of the National Cancer Institute (NCI) workshop.[27] High-frequency MSI (MSI-H) was defined as the alterations of microsatellite repeat were found in more than 40% of examined markers or in 2 or more NCI-recommended markers. Low-frequency MSI (MSI-L) was defined as the alterations in less than 40% or only one NCI-recommended marker. If no alterations of any examined markers were found, tumors were defined as microsatellite stable (MSS). In this study, we defined MSI-H as MSI-positive (MSI^+), and both MSI-L and MSS as MSI-negative (MSI^-), because only the MSI-H phenotype in sporadic CRCs is associated with true MMR defects and distinctive clinicopathologic features.[28,29] For the precision of MSI status, we reexamined all MSI^+ samples by pentaplex PCR method using 5 quasimonomorphic mononucleotide repeats, because this method has been reported to be simpler to use and show higher sensitivity and specificity.[30]

Analysis of methylation status of hMLH1 *promoter region*

Analysis of methylation status of *hMLH1* gene was performed by Na-bisulfite treatment and PCR single-strand conformation polymorphism (SSCP) analysis (BiPS) as described previously.[21] In brief, 5 sets of primers comprising the whole CpG sites within the *hMLH1* promoter region were prepared (Fig. 1), and methylated and unmethylated DNA amplicons were separated through SSCP analysis. When the bands showed mobility shifts, they were cut from the gels and subsequently sequenced directly by use of an ABI 310 PRISM Genetic Analyzer. Primer sequences and PCR conditions were utilized as reported previously.[21] The methylation patterns were defined as full methylation if all the CpG sites within the promoter regions showed methylation; as partial methylation if some CpG sites in the upstream region showed methylation; and as nonmethylation if no CpG sites in the region showed methylation.

KRAS *mutation analysis*

KRAS mutations were analyzed by direct sequencing at codons 12 and 13 of *KRAS* by using its genomic DNA. First, a flanking PCR product of 179 bp was amplified (annealing temperature was 58°C) using the primers 5′-AGGCCTGCTGAAAATGACTGAATA-3′ (sense) and 5′-CTGTATCAAAGAATGGTCCTGCAC-3′ (antisense). The resulting fragment was then used as a template to amplify a 114 bp fragment, including codons 12 and 13 using the primers 5′-AAAATGACTGAATATAAACTTGTGG-3′ (sense) and 5′-CTCTATTGTTGGATCATATTCGTC-3′ (antisense; annealing temperature was 50°C). The PCR product was sequenced by the same method as in the *BRAF* mutation analysis.

β-catenin *mutation analysis*

Mutations in *β-catenin* were analyzed by direct sequencing at its exon 3, in which the majority of mutation hot spots were included. The PCR primers were 5′-GATTTGATGGAGTTGGACATGG-3′ (sense) and 5′-TGTTCTTGAGTGAAGGACTGAG-3′ (antisense; annealing temperature was 63°C). The direct sequencing of the PCR product was performed by the same method as in the *BRAF* mutation analysis.

Immunohistochemical analysis

Immunohistochemical analysis for both hMLH1 and hMSH2 expression was performed on all MSI^+ tumor samples as described previously.[26]

Statistical analysis

Statistical analyses for variable results were performed by Fisher's exact test and Student's *t*-test. Probability values below 0.05 were considered to be statistically significant (StatView J 5.0 software, Abacus Concepts, Berkeley, CA).

RESULTS

Clinicopathologic features of patients with BRAF *mutations*

We identified 16 patients whose CRCs showed *BRAF* mutations (Table I). All the mutations resulted in a V599E substitution in the

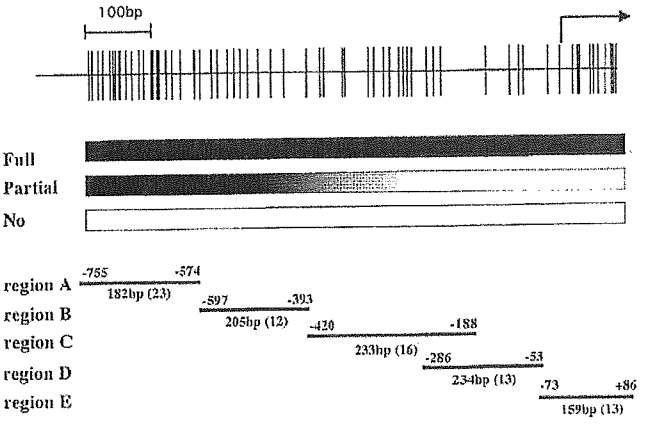

FIGURE 1 – Top: Schematic presentation of the *MLH1* promoter region. Middle: Full methylation (all CpG sites in regions A–E show methylation), partial methylation (some CpG sites in upstream region show methylation) and nonmethylation (no CpG site shows methylation). Bottom: Design of the PCR primers and the PCR products for regions A–E. Their positions relative to the adenine residue at the start codon and the size of the amplified DNA fragments are shown. Numbers in parenthesis indicate the number of CpG sites within each region.

BRAF protein (Fig. 2). None of the cases had *BRAF* mutations in the normal colonic mucosa positioned far away from the cancer area, implying that the *BRAF* mutations should be a somatic event. The mean age of cancer onset in the patients with *BRAF* mutations was older than those without *BRAF* mutations, although the difference was not statistically significant: 73.1 ± 10.5 years compared with 62.5 ± 12.5 years ($p = 0.06$, Student's *t*-test; Table II). Gender distribution was also different between these 2 groups, with females comprising 75% (12/16) of the *BRAF* mutation group and 48% (59/124) of the nonmutation group ($p = 0.06$, Fisher's exact test; Table II). The tumor with *BRAF* mutation cases was more frequently located in the proximal colon (94%; 15/16) than that with nonmutation ones (37%; 46/124; $p < 0.0001$, Fisher's exact test; Table II).

BRAF *mutations and MSI status*

BRAF mutations were found in 43% (12/28) of MSI^+ CRCs and 4% (4/112) of MSI^- CRCs ($p < 0.0001$, Fisher's exact test; Table III).

BRAF *mutations and MMR protein expression*

BRAF mutations were more common in the tumors showing reduced hMLH1 protein expression (58%; 11/19) than those showing reduced hMSH2 expression (0%; 0/6; $p = 0.02$, Fisher's exact test; Table IV).

BRAF *mutations and* hMLH1 *promoter methylation status*

BRAF mutations were found in 69% (11/16) of full methylation, 4% (2/45) of partial methylation and 4% (3/79) of nonmethylation (Table V). The ratio of *BRAF* mutations was statistically significant between full and partial as well as between full and none ($p < 0.0001$, Fisher's exact test).

KRAS *mutations*

KRAS mutations were identified in 38 cases. Two cases with *KRAS* mutations were in MSI^+ (7%; 2/28) and 36 cases were in MSI^- (32%; 36/112; $p = 0.008$, Fisher's exact test; Table III). Regarding the methylation status, *KRAS* mutations were not found

TABLE I – ALL CRC CASES WITH *BRAF* MUTATIONS

Patient no.	Age (yr)	Gender	Site	MSI	*hMLH1* methylation	*BRAF* amino acid	*KRAS*	β-*catenin*	Dukes' stage	Histologic grade
225	83	F	P	+	Full	V599E	Wild	Wild	C	Well
263	86	F	P	+	Full	V599E	Wild	Wild	B	Moderate
268	85	F	P	+	Full	V599E	Wild	Wild	B	Poor
280	83	F	P	+	Full	V599E	Wild	Wild	C	Well
305	74	M	P	+	Full	V599E	Wild	Wild	B	Poor
318	76	F	P	+	Full	V599E	Wild	Wild	B	Well
336	68	M	P	+	Full	V599E	Wild	Wild	B	Mucinous
413	69	F	P	+	Full	V599E	Wild	Wild	B	Well
416	76	F	P	+	Full	V599E	Wild	Wild	B	Mucinous
479	74	F	P	+	Full	V599E	Wild	Wild	B	Moderate
507	64	M	P	+	Full	V599E	Wild	Wild	A	Moderate
274	81	M	D	−	Partial	V599E	Wild	Wild	B	Moderate
328	52	F	P	−	Partial	V599E	Wild	Wild	B	Moderate
293	70	F	P	−	Non	V599E	Wild	Wild	D	Mucinous
384	77	F	P	+	Non	V599E	Wild	Wild	A	Poor
509	51	F	P	−	Non	V599E	Wild	Wild	C	Poor

P, proximal colon; D, distal colon; Full, full methylation; Partial, partial methylation; Non, nonmethylation; Well, well-differentiated adenocarcinoma; Mod, moderately differentiated adenocarcinoma; Poor, poorly differentiated adenocarcinoma; Muc, mucinous carcinoma.

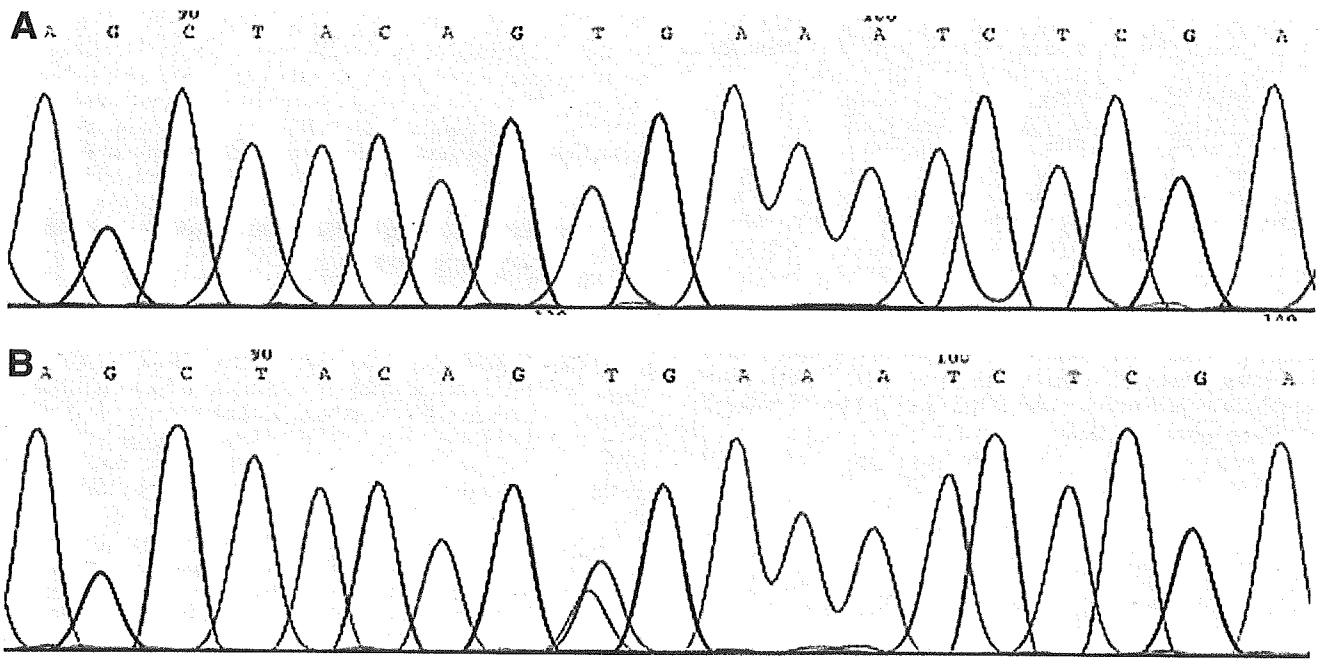

FIGURE 2 – (*a*) Representative sequence chromatographs from *BRAF* exon 15 showing wild type. (*b*) T1796A transversion resulting in a V599E substitution.

TABLE II – CLINICOPATHOLOGIC FEATURES OF *BRAF* MUTATION CASES

	BRAF mutation (n = 16) (%)	Non-*BRAF* mutation (n = 124) (%)	P-value
Age (yr)	73.1 ± 10.5	62.5 ± 12.5	0.06
Gender			0.06
Male	4 (25)	65 (52)	
Female	12 (75)	59 (48)	
Tumor site			< 0.0001
Proximal	15 (94)	46 (37)	
Distal	1 (6)	78 (63)	
Dukes' stage			0.07
A/B	12 (75)	59 (50)	
C/D	4 (25)	59 (50)	
Histologic grade			0.0008
Well/moderate	9 (56)	109 (92)	
Poor/mucinous	7 (44)	10 (8)	

Well, well-differentiated adenocarcinoma; moderate, moderately differentiated adenocarcinoma; Poor, poorly differentiated adenocarcinoma; mucinous, mucinous carcinoma.

TABLE III – MSI STATUS AND MUTATIONS OF *BRAF*, *KRAS* AND β-*CATENIN*

MSI status	*BRAF* mutation (%)	*KRAS* mutation (%)	β-*catenin* mutation (%)
MSI$^+$	42.9 (12/28)[a]	7.1 (2/28)[b]	7.1 (2/28)
MSI$^-$	3.6 (4/112)[a]	32.1 (36/112)[b]	2.7 (3/112)
Total	11.4 (16/140)	27.1 (38/140)	3.6 (5/140)

[a]Fisher's exact test, $p < 0.0001$.–[b]Fisher's exact test, $p = 0.008$.

TABLE IV – *BRAF* MUTATION AND MMR PROTEIN EXPRESSION

	Number of cases	*BRAF* mutation (%)
hMLH1-deficient	19	57.9 (11/19)[a]
hMSH2-deficient	6	0 (0/6)[a]

[a]Fisher's exact test, $p = 0.02$.

TABLE V – *hMLH1* METHYLATION STATUS AND MUTATIONS OF *BRAF*, *KRAS* AND β-*CATENIN*

hMLH1 methylation status	*BRAF* mutation (%)	*KRAS* mutation (%)	β-*catenin* mutation (%)
Full methylation	68.8 (11/16)[a,b]	0 (0/16)[c,d]	0 (0/16)
Partial methylation	4.4 (2/45)[a]	37.8 (17/45)[c]	0 (0/45)
Nonmethylation	3.8 (3/79)[b]	26.6 (21/79)[d]	6.3 (5/79)
Total	11.4 (16/140)	27.1 (38/140)	3.6 (5/140)

[a]Fisher's exact test, $P < 0.0001$.–[b]Fisher's exact test, $P < 0.0001$.–[c]Fisher's exact test, $P = 0.003$.–[d]Fisher's exact test, $P = 0.02$.

(0%; 0/16) in any of the full methylation cases, but were found in 17 of the partial methylation patients (38%; 17/45) and 21 of the nonmethylation group (26.6%; 21/79), which was consistent with our previous results[21] (Table V). The ratio of *KRAS* mutations was significantly different between full and partial and between full and none cases (p = 0.003 and 0.02, respectively, Fisher's exact test). None of the cases with *BRAF* mutations exhibited *KRAS* mutations simultaneously.

β-catenin *mutations*

β-catenin mutations were found in 5 cases. Two cases were in MSI$^+$ (7%; 2/28) and 3 cases were in MSI$^-$ (3%; 3/112; p = 0.26, Fisher's exact test; Table III). However, none of the cases with full or partial methylation showed *β-catenin* mutations, and there were no cases exhibiting both *BRAF* and *β-catenin* mutations simultaneously (Table V).

DISCUSSIONS

The MAPK pathway plays a crucial role in the signal transduction of many hormones, growth factors and differentiation factors.[31,32] At the level of MAPKKKs, several RAF family members exist, that is, ARAF, BRAF and RAF1 with divergent tissue specificity and upstream regulation.[33] The 3 proteins are thought to have uneven ability to activate MEK, and BRAF has been identified as the major MEK activator.[32]

Recently, *BRAF* activating mutations were observed in some proportion of human carcinomas, especially in melanoma, lung cancer, as well as colon cancer.[5–7] *BRAF* gene was therefore supposed to be a novel protooncogene that might contribute to the tumorigenesis in these types of transformed cells. Interestingly, the mutational spots of *BRAF* gene cluster within the activation segment (exon 15) and the G-loop (exon 11) of the kinase domain, which are highly conserved among serine/threonine kinases throughout evolution.[5] Activating mutations in these hot spots are supposed to increase its kinase activity and subsequently urge to phosphorylate the downstream kinase, MEK. V599 is the major site of point mutations in the BRAF protein and V599E acidic substitution has been commonly found in melanoma, colon cancer and ovarian cancer cells.[5] Intriguingly, the tumors with BRAF^{V599E} showed no *KRAS* mutations simultaneously, although non-V599E cases were sometimes coincident with *KRAS* mutations.[5,10,34] It has been hypothesized therefore that V599E might mimic the phosphorylation of T598 of BRAF that constitutes the natural activation mechanism of this protein. Because of its potent kinase activity, BRAF with this type of mutation might have no need to depend on RAS for the initiation of the MAP kinase pathway activation.

In our series of sporadic CRCs, 28 cases showed MSI$^+$, in which 19 were with hMLH1 deficiency and 6 were with hMSH2 deficiency. *BRAF* mutations were more frequent in MSI$^+$ CRCs than in MSI$^-$ CRCs (43%, 12/28 *vs.* 4%, 4/112; $p < 0.0001$). This result was nearly consistent with that in the previous report.[10] Interestingly, *BRAF* mutations were more frequent in hMLH1-deficient cases than hMSH2-deficient ones (58%, 11/19 *vs.* 0%, 0/6; p = 0.02). It has been widely accepted that MSI in sporadic CRCs commonly results from epigenetic silencing of *hMLH1* gene, secondary to its promoter methylation, and 70–90% of MSI$^+$ CRCs indeed show hypermethylation of the *hMLH1* gene.[15,21,35] Moreover, extensive methylation of *hMLH1* promoter is closely correlated with hMLH1 inactivation.[21] Therefore, we have examined the frequency of *BRAF* mutations with regard to the methylation status of *hMLH1* promoter region. Amazingly, *BRAF* mutations were extremely frequent in the cases with full methylation compared to those without full methylation (69%, 11/16 *vs.* 4%, 5/124; $p < 0.0001$). As generally seen in the cases with *hMLH1* methylation, the CRCs with *BRAF* mutations were more frequent in older females, commonly located in the proximal colon, and showed the histopathology of mucinous or poor differentiation. Our data suggest that the activating mutation of *BRAF* may be highly associated with an extensive methylation of *hMLH1* gene.

In a recent study, we proposed that the shift of methylation status from partial to full might be critical in the tumorigenesis of right-sided sporadic CRCs with MSI, because more than half of the cases with full methylation showed partial methylation in their normal mucosa far from the tumor.[21] However, the cancers with partial methylation not yet reaching full methylation showed distinct clinical and biologic features from those with full methylation, with relatively high frequency in the alterations of *KRAS*/*p53*.[22] In this study, *BRAF* mutations were less frequent in the cases with partial methylation compared to those with full methylation (4%, 2/45 *vs.* 69%, 11/16; $p < 0.0001$). We state that partial methylation is not generally the true pathogenic methylation status of *hMLH1* gene.

In our study, all the mutations of *BRAF* resulted in V599E substitutions (T-to-A transversion at nucleotide 1796). Rajago-

palan *et al.*[10] reported that all but one of the 15 *BRAF* mutations in MMR-deficient cases resulted in V599E. O^6-methylguanine DNA methyltransferase (MGMT) is a DNA repair protein and MGMT epigenetic inactivation by its promoter hypermethylation is supposed to cause G-to-A transition mutation in *KRAS* and G:C-to-A:T transition mutation in *p53*. Indeed, 71% cases with *KRAS* and *p53* mutations showed hypermethylation of *MGMT*.[36,37] Therefore, it might be possible that inactivation of an anonymous DNA-repair gene by promoter hypermethylation has an association with A-to-T transition mutation in *BRAF* gene.

Yuen *et al.*[34] have reported that there are many similarities between the phenotypic patterns of CRCs with *KRAS* and *BRAF* mutations. However, they showed that the cases with *BRAF* mutations differ from those with *KRAS* mutations in the Dukes' stage. Consistent with their results, the cases with *BRAF* mutations in our study were more common with Dukes' A/B grades than with Dukes' C/D, although the difference was not statistically significant ($p = 0.07$, Fisher's exact test). Moreover, the patients with *BRAF* mutations were approximately 13 years older than those with *KRAS* mutations (data not shown). Therefore, we speculate that the CRCs with *BRAF* mutations may belong to a clinical entity distinct from one of CRCs with *KRAS* mutations.

In melanoma cells as well as MSI^+ CRC cells, high frequency of *β-catenin* and *BRAF* mutations have been reported.[19,23–25] In this study, *β-catenin* mutations were uncommon in both MSI^+ (7%; 2/28) and MSI^- (3%; 3/112), as reported previously by Jass *et al.*[29] Moreover, none of our cases with full or partial methylation showed *β-catenin* mutations. There were no cases harboring *BRAF* and *β-catenin* mutations simultaneously, implying that *β-catenin* mutation may have no association with *hMLH1* hypermethylation with regard to CRC carcinogenesis.

We previously proposed that extensive methylation of *hMLH1* promoter might play a crucial role in tumorigenesis in the proximal colon.[21] In this study, we additionally demonstrated that the activating mutations of *BRAF* might take part in the carcinogenesis of sporadic CRCs with *hMLH1* hypermethylation in the proximal colon, independently of KRAS activation. However, one question remains to be addressed. At which stage does BRAF activation contribute to malignant transformation of colon epithelial cells? Hyperplastic polyps and serrated adenomas in the right-sided colon show high frequency of *hMLH1* hypermethylation, and these lesions have been presumed to be premalignant lesions of right-sided CRCs with MSI.[29] It would be interesting to examine whether the majority of such hyperplastic polyps and serrated adenomas already have *BRAF* mutations. If most of the CRCs with extensive methylation are associated with $BRAF^{V599E}$, such subtype would be a good target for novel anticancer drugs acting on the MAPK pathway.[38,39]

ACKNOWLEDGEMENTS

The authors thank the staff of the Division of Functional Genomics, Jichi Medical School, for their helpful advice.

REFERENCES

1. Kinzler KW, Vogelstein B. Lessons from hereditary colorectal cancer. Cell 1996;87:159–70.
2. Aaltonen LA, Peltomaki P, Leach FS, Sistonen P, Pylkkanen L, Mecklin JP, Jarvinen H, Powell SM, Jen J, Hamilton SR, Petersen GM, Kinzler KW, et al. Clues to the pathogenesis of familial colorectal cancer. Science 1993;260:812–6.
3. Bos JL, Fearon ER, Hamilton SR, Verlaan-de Vries M, van Boom JH, van der Eb AJ, Vogelstein B. Prevalence of ras gene mutations in human colorectal cancers. Nature 1987;327:293–7.
4. Forrester K, Almoguera C, Han K, Grizzle WE, Perucho M. Detection of high incidence of K-ras oncogenes during human colon tumorigenesis. Nature 1987;327:298–303.
5. Davies H, Bignell GR, Cox C, Stephens P, Edkins S, Clegg S, Teague J, Woffendin H, Garnett MJ, Bottomley W, Davis N, Dicks E, et al. Mutations of the BRAF gene in human cancer. Nature 2002;417:949–54.
6. Pollock PM, Meltzer PS. A genome-based strategy uncovers frequent BRAF mutations in melanoma. Cancer Cell 2002;2:5–7.
7. Brose MS, Volpe P, Feldman M, Kumar M, Rishi I, Gerrero R, Einhorn E, Herlyn M, Minna J, Nicholson A, Roth JA, Albelda SM, et al. BRAF and RAS mutations in human lung cancer and melanoma. Cancer Res 2002;62:6997–7000.
8. Vojtek AB, Der CJ. Increasing complexity of the Ras signaling pathway. J Biol Chem 1998;273:19925–8.
9. Magee T, Marshall C. New insights into the interaction of Ras with the plasma membrane. Cell 1999;98:9–12.
10. Rajagopalan H, Bardelli A, Lengauer C, Kinzler KW, Vogelstein B, Velculescu VE. Tumorigenesis: RAF/RAS oncogenes and mismatch-repair status. Nature 2002;418:934.
11. Aaltonen LA, Peltomaki P, Mecklin JP, Jarvinen H, Jass JR, Green JS, Lynch HT, Watson P, Tallqvist G, Juhola M. Replication errors in benign and malignant tumors from hereditary nonpolyposis colorectal cancer patients. Cancer Res 1994;54:1645–8.
12. Fishel R, Lescoe MK, Rao MR, Copeland NG, Jenkins NA, Garber J, Kane M, Kolodner R. The human mutator gene homolog MSH2 and its association with hereditary nonpolyposis colon cancer. Cell 1993; 75:1027–38.
13. Bronner CE, Baker SM, Morrison PT, Warren G, Smith LG, Lescoe MK, Kane M, Earabino C, Lipford J, Lindblom A, Tannergard P, Bollag RJ, et al. Mutation in the DNA mismatch repair gene homologue hMLH1 is associated with hereditary non-polyposis colon cancer. Nature 1994;368:258–61.
14. Kane MF, Loda M, Gaida GM, Lipman J, Mishra R, Goldman H, Jessup JM, Kolodner R. Methylation of the hMLH1 promoter correlates with lack of expression of hMLH1 in sporadic colon tumors and mismatch repair-defective human tumor cell lines. Cancer Res 1997; 57:808–11.
15. Cunningham JM, Christensen ER, Tester DJ, Kim CY, Roche PC, Burgart LJ, Thibodeau SN. Hypermethylation of the hMLH1 promoter in colon cancer with microsatellite instability. Cancer Res 1998;58:3455–60.
16. Veigl ML, Kasturi L, Olechnowicz J, Ma AH, Lutterbaugh JD, Periyasamy S, Li GM, Drummond J, Modrich PL, Sedwick WD, Markowitz SD. Biallelic inactivation of hMLH1 by epigenetic gene silencing, a novel mechanism causing human MSI cancers. Proc Natl Acad Sci USA 1998;95:8698–702.
17. Kuismanen SA, Holmberg MT, Salovaara R, Schweizer P, Aaltonen LA, de La Chapelle A, Nystrom-Lahti M, Peltomaki P. Epigenetic phenotypes distinguish microsatellite-stable and -unstable colorectal cancers. Proc Natl Acad Sci USA 1999;96:12661–6.
18. Malkhosyan SR, Yamamoto H, Piao Z, Perucho M. Late onset and high incidence of colon cancer of the mutator phenotype with hypermethylated hMLH1 gene in women. Gastroenterology 2000;119:598.
19. Young J, Simms LA, Biden KG, Wynter C, Whitehall V, Karamatic R, George J, Goldblatt J, Walpole I, Robin SA, Borten MM, Stitz R, et al. Features of colorectal cancers with high-level microsatellite instability occurring in familial and sporadic settings: parallel pathways of tumorigenesis. Am J Pathol 2001;159:2107–16.
20. Hawkins N, Norrie M, Cheong K, Mokany E, Ku SL, Meagher A, O'Connor T, Ward R. CpG island methylation in sporadic colorectal cancers and its relationship to microsatellite instability. Gastroenterology 2002;122:1376–87.
21. Miyakura Y, Sugano K, Konishi F, Ichikawa A, Maekawa M, Shitoh K, Igarashi S, Kotake K, Koyama Y, Nagai H. Extensive methylation of hMLH1 promoter region predominates in proximal colon cancer with microsatellite instability. Gastroenterology 2001;121:1300–9.
22. Miyakura Y, Sugano K, Konishi F, Fukayama N, Igarashi S, Kotake K, Matsui T, Koyama Y, Maekawa M, Nagai H. Methylation profile of the MLH1 promoter region and their relationship to colorectal carcinogenesis. Genes Chromosomes Cancer 2003;36:17–25.
23. Sparks AB, Morin PJ, Vogelstein B, Kinzler KW. Mutational analysis of the APC/beta-catenin/Tcf pathway in colorectal cancer. Cancer Res 1998;58:1130–4.
24. Shitoh K, Furukawa T, Kojima M, Konishi F, Miyaki M, Tsukamoto T, Nagai H. Frequent activation of the beta-catenin-Tcf signaling pathway in nonfamilial colorectal carcinomas with microsatellite instability. Genes Chromosomes Cancer 2001;30:32–7.
25. Mirabelli-Primdahl L, Gryfe R, Kim H, Millar A, Luceri C, Dale D, Holowaty E, Bapat B, Gallinger S, Redston M. Beta-catenin mutations are specific for colorectal carcinomas with microsatellite instability but occur in endometrial carcinomas irrespective of mutator pathway. Cancer Res 1999;59:3346–51.
26. Furukawa T, Konishi F, Masubuchi S, Shitoh K, Nagai H, Tsukamoto T. Densely methylated MLH1 promoter correlates with decreased mRNA expression in sporadic colorectal cancers. Genes Chromosomes Cancer 2002;35:1–10.

27. Boland CR, Thibodeau SN, Hamilton SR, Sidransky D, Eshleman JR, Burt RW, Meltzer SJ, Rodriguez-Bigas MA, Fodde R, Ranzani GN, Srivastava S. A National Cancer Institute workshop on microsatellite instability for cancer detection and familial predisposition: development of international criteria for the determination of microsatellite instability in colorectal cancer. Cancer Res 1998;58:5248–57.
28. Konishi M, Kikuchi-Yanoshita R, Tanaka K, Muraoka M, Onda A, Okumura Y, Kishi N, Iwama T, Mori T, Koike M, Ushio K, Chiba M, et al. Molecular nature of colon tumors in hereditary nonpolyposis colon cancer, familial polyposis, and sporadic colon cancer. Gastroenterology 1996;111:307–17.
29. Jass JR, Biden KG, Cummings MC, Simms LA, Walsh M, Schoch E, Meltzer SJ, Wright C, Searle J, Young J, Leggett BA. Characterisation of a subtype of colorectal cancer combining features of the suppressor and mild mutator pathways. J Clin Pathol 1999;52:455–60.
30. Suraweera N, Duval A, Reperant M, Vaury C, Furlan D, Leroy K, Seruca R, Iacopetta B, Hamelin R. Evaluation of tumor microsatellite instability using five quasimonomorphic mononucleotide repeats and pentaplex PCR. Gastroenterology 2002;123:1804–11.
31. Kolch W. Meaningful relationships: the regulation of the Ras/Raf/MEK/ERK pathway by protein interactions. Biochem J 2000;351(Pt 2):289–305.
32. Peyssonnaux C, Eychene A. The Raf/MEK/ERK pathway: new concepts of activation. Biol Cell 2001;93:53–62.
33. Barnier JV, Papin C, Eychene A, Lecoq O, Calothy G. The mouse B-raf gene encodes multiple protein isoforms with tissue-specific expression. J Biol Chem 1995;270:23381–9.
34. Yuen ST, Davies H, Chan TL, Ho JW, Bignell GR, Cox C, Stephens P, Edkins S, Tsui WW, Chan AS, Futreal PA, Stratton MR, et al. Similarity of the phenotypic patterns associated with BRAF and KRAS mutations in colorectal neoplasia. Cancer Res 2002;62:6451–5.
35. Herman JG, Umar A, Polyak K, Graff JR, Ahuja N, Issa JP, Markowitz S, Willson JK, Hamilton SR, Kinzler KW, Kane MF, Kolodner RD, et al. Incidence and functional consequences of hMLH1 promoter hypermethylation in colorectal carcinoma. Proc Natl Acad Sci USA 1998;95:6870–5.
36. Esteller M, Toyota M, Sanchez-Cespedes M, Capella G, Peinado MA, Watkins DN, Issa JP, Sidransky D, Baylin SB, Herman JG. Inactivation of the DNA repair gene O6-methylguanine-DNA methyltransferase by promoter hypermethylation is associated with G to A mutations in K-ras in colorectal tumorigenesis. Cancer Res 2000;60:2368–71.
37. Esteller M, Risques RA, Toyota M, Capella G, Moreno V, Peinado MA, Baylin SB, Herman JG. Promoter hypermethylation of the DNA repair gene O(6)-methylguanine-DNA methyltransferase is associated with the presence of G:C to A:T transition mutations in p53 in human colorectal tumorigenesis. Cancer Res 2001;61:4689–92.
38. Lee JT Jr, McCubrey JA. The Raf/MEK/ERK signal transduction cascade as a target for chemotherapeutic intervention in leukemia. Leukemia 2002;16:486–507.
39. Sebolt-Leopold JS. Development of anticancer drugs targeting the MAP kinase pathway. Oncogene 2000;19:6594–9.

High-throughput screening of genome fragments bound to differentially acetylated histones

Ruri Kaneda[1,2], Minoru Toyota[3], Yoshihiro Yamashita[1], Koji Koinuma[1], Young Lim Choi[1], Jun Ota[1,4], Hiroyuki Kisanuki[1], Madoka Ishikawa[1], Shuji Takada[1], Kazuyuki Shimada[2] and Hiroyuki Mano[1,4,*]

Divisions of [1]Functional Genomics, and [2]Cardiology, Jichi Medical School, 3311-1 Yakushiji, Kawachigun, Tochigi 329-0498, Japan
[3]Department of Molecular Biology, Cancer Research Institute, Sapporo Medical University, Sapporo 060-8556, Japan
[4]CREST, Japan Science and Technology Agency, Saitama 332-0012, Japan

Although acetylation-deacetylation of histones contributes to regulation of gene expression, few methods have been available to determine the whole-genome histone acetylation profile in specific cells or tissues. We have now developed a genome-wide screening method, differential chromatin scanning (DCS), to isolate genome fragments embedded in histones subject to differential acetylation. This DCS screening was applied to a human gastric cancer cell line incubated with or without an inhibitor of histone deacetylase (HDAC) activity, resulting in the rapid identification of more than 250 genome fragments. Interestingly, a number of cancer-related genes were revealed to be the targets of HDAC in the cancer cells, including those for tumour protein 73 and cell division cycle 34. Such differential acetylation of histone was also shown to be linked to the regulation of transcriptional activity of the corresponding genes. Among the isolated genome fragments, 94% (32/34) of them were confirmed to be bound to differentially acetylated histones, and the genes corresponding to 78% (7/9) of them exhibited differential transcriptional activity consistent with the level of histone acetylation. With its high fidelity, the DCS method should open a possibility to rapidly compare the genome-wide histone acetylation profiles and to provide novel insights into molecular carcinogenesis.

Introduction

The genomic DNA of eukaryotes is compactly packaged by complexation with histones, rendering it physically difficult for the nuclear machinery responsible for DNA transcription or replication to access the DNA. However, this three-dimensional structure of genomic DNA is subject to dynamic and rapid regulation by various chemical modifications of the DNA itself or of its surrounding histones. These epigenetic modifications include DNA methylation as well as histone acetylation, methylation, and phosphorylation (Baylin & Herman 2000; Burgess-Beusse *et al.* 2002; van Leeuwen & Gottschling 2002).

Acetylation of histones is mediated by histone acetyltransferases (HATs) and takes place on the ε-amino group of conserved lysine residues located in the NH_2-terminal tail of core histones (Carrozza *et al.* 2003). Such histone modification is tightly linked to transcriptional regulation by either chromatin remodeling or the provision of binding sites for other proteins. HAT activity in cells is rapidly counteracted by the activity of histone deacetylases (HDACs) (Verdin *et al.* 2003), with the result that the turnover time of histone acetylation is as short as a few minutes (Waterborg 2002).

The importance of histone acetylation in the regulation of gene expression has been demonstrated for a variety of cellular processes including cell differentiation, cell cycle progression, DNA repair, and carcinogenesis (Kouzarides 1999; Yasui *et al.* 2003). Furthermore, a histone acetylation profile (HAP) of a certain type of acute myeloid leukaemia was shown to be directly related to the sensitivity of the malignancy to chemotherapeutic agents (Grignani *et al.* 1998; Lin *et al.* 1998). Elucidation of the HAP of human malignancies may therefore provide a basis for novel approaches to cancer treatment. This notion is supported by the observation that inhibitors of HDAC activity are effective in the treatment of haematological malignancies such as multiple myeloma and myelodysplastic syndrome (Gore *et al.* 2001; Catley

Communicated by: Fuyuki Ishikawa
**Correspondence*: E-mail: hmano@jichi.ac.jp

DOI: 10.1111/j.1365-2443.2004.00804.x

et al. 2003). The means to establish a genome-wide HAP have been lacking, however (Gabrielli *et al.* 2002).

To characterize the HAP of any given cell or tissue type, we have now developed a new screening method, termed differential chromatin scanning (DCS). Application of the DCS method to a human gastric cancer cell line has readily identified hundreds of target fragments of histone deacetylase (HDAC), including a number of cancer-related genes such as *tumour protein p73* (*TP73*), *cell division cycle 34* (*CDC34*), and *bone morphogenetic protein 7* (*BMP7*).

With its high fidelity, DCS enables us a genome-wide screening of DNA fragments embedded in histones with differential acetylation level between a given pair of samples.

Results

The DCS method

The DCS procedure is schematically shown in Fig. 1. We verified the screening ability of this method by identifying HDAC targets in the genome of the human gastric cancer cell line MKN28. The cells were treated with trichostatin A (TSA), a specific inhibitor of HDAC activity, for use as a 'tester' sample, whereas MKN28 cells not subjected to TSA treatment were used as a 'driver'. Inhibition of HDAC activity by TSA would be expected to increase the acetylation level of target histones compared with that apparent in the driver sample. We thus attempted to rapidly isolate genomic fragments bound to histones that were acetylated only in the tester sample.

After the cross-linking of DNA to histones with the use of formaldehyde, both tester and driver cells were separately lysed and subjected to mild DNA shearing by sonication for a short period. Complexes of DNA and acetylated histones were then specifically immunoprecipitated with antibodies to acetylated histone H3, after which the DNA fragments were released from such complexes into solution.

The nonspecific binding of residual RNA was minimized by treating the DNA solution with RNase A, and the DNA fragments were then rendered blunt-ended. The DNA was digested maximally with *RsaI* to obtain fragments with a relatively uniform size of several hundred base pairs. A TAG adaptor was ligated to both ends of the DNA fragments, and subsequent PCR amplification with a TAG primer yielded amplicons with an *XmaI*/*SmaI* site at each end.

The tester DNA was then digested with *XmaI* (thereby generating cohesive ends), whereas the driver DNA was digested with *SmaI* (generating blunt ends). The tester DNA was ligated with the first subtraction adaptor (Toyota *et al.* 1999) through its cohesive ends and was then annealed to an excess amount of the driver DNA. Under this condition, DNA fragments present only in the tester sample undergo self-annealing and thereby generate a binding site for the first subtraction primer at both ends. Subsequent PCR amplification with this primer thus selectively amplified the tester-specific DNA fragments.

To exclude DNA fragments that possess endogenous (probably nonspecific) binding sites for the first subtraction primer, we digested the first subtraction products with *XmaI* and ligated the resulting molecules with the second subtraction adaptor. A second round of subtraction amplification was then performed with the second subtraction primer, yielding DNA fragments that were associated with acetylated histones specifically in the tester cells.

HDAC targets in a cancer cell line

From the products of the second round of subtraction PCR, we randomly selected 288 DNA fragments and determined their nucleotide sequence. The size of the genome fragments was ≥ 50 bp in 265 clones (mean size, ~270 bp), and these DNA sequences were subjected to subsequent analyses. The sequences were first screened with the BLAT search program (Kent 2002) against the nucleotide sequence database assembled as of July 2003 by the Genome Bioinformatics Group of the University of California at Santa Cruz (http://genome.ucsc.edu/). Among the 265 DNA fragments examined, 200 sequences showed > 95% identity to the human genome sequence and 198 of these were located either within a protein-coding gene (demonstrated or predicted) or in the vicinity (within 5 kbp) of such a gene (Table 1 and Table S1).

To verify the fidelity of the tester-specific amplification by our DCS method, we chose 34 DNA fragments and quantified their abundance in the immunoprecipitates prepared from both tester and driver cells with the antibodies to acetylated histone H3. The amount of each DNA fragment relative to that of the *glyceraldehyde-3-phosphate dehydrogenase* (*GAPDH*) gene was determined by quantitative real-time polymerase chain reaction (PCR). As shown in Table 1, selective amplification by DCS was proved to be highly reliable, with 32 out of 34 clones exhibiting tester-specific precipitation (tester/driver ratio ≥ 1.5).

TP73 as a target of HDAC

Interestingly, certain of these 32 clones corresponded to sequences either within or close to human cancer-related

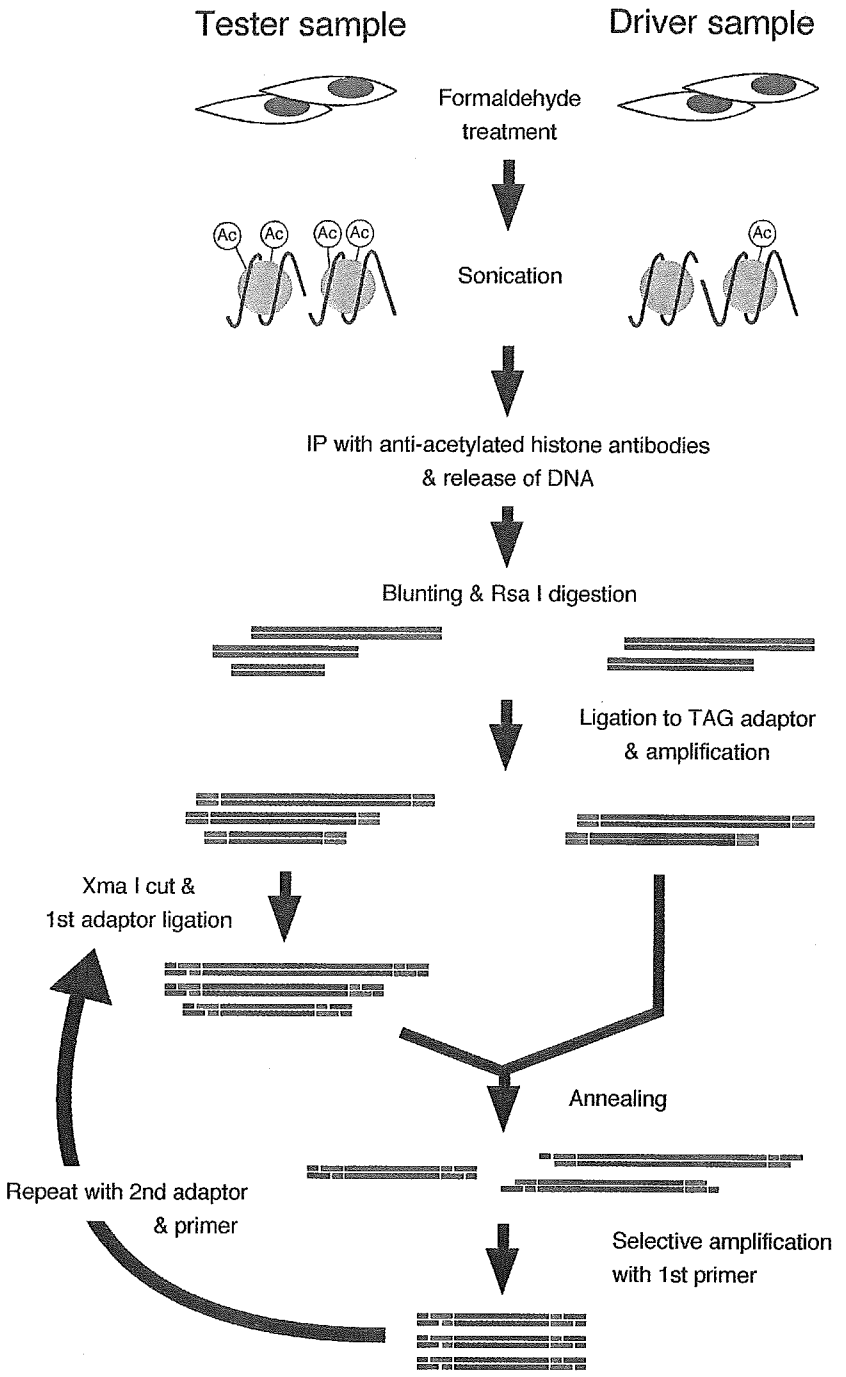

Figure 1 The DCS method. DNA fragments bound to acetylated (Ac) histones are purified by immunoprecipitation (IP) and subjected to TAG adaptor ligation (green bars) and PCR amplification. The tester DNA is then digested with *Xma*I, ligated to the first subtraction adaptor (red bars), and annealed with an excess amount of the driver DNA. Given that only the tester-specific fragments self-anneal, PCR with the first subtraction primer selectively amplifies these fragments. The products are subjected to a second round of subtraction PCR with the second subtraction adaptor and primer to ensure the fidelity of subtraction.

genes, including those for TP73, CDC34, and BMP7. One of the clones (10sBKR_D10) was, for instance, mapped to a region located ~1.2 kbp downstream of the last exon of *TP73* (GenBank accession number, NM_005427) (Fig. 2A). TP73 is a close homologue of a well-known tumour suppressor, TP53. The *TP73* gene is localized at 1p36 locus which is subject to recurrent loss of heterozygosity in various human cancers (Kaghad *et al.* 1997). An array of isoforms for TP73 are generated *in vivo* through alternative splicing mechanism of its mRNA, and those forms exert a variety of (sometimes, opposite) actions on tumour growth (Benard *et al.* 2003).

Thus, it was intriguing to examine whether, in this gastric caner cell line, histone acetylation takes place

Table 1 Genome fragments isolated through the DCS screening

Clone ID	Chromosome position	Tester/driver DNA ratio	GenBank accession no.	Tester/driver mRNA ratio	Annotation
10sBKR_A02	20q13.31	4.79	NM001719		Homo sapiens, bone morphogenetic protein 7 (osteogenic protein 1)
10sBKR_A03	11p15.5	3.66	AK056774		Homo sapiens gene duplee encoding H19
10sBKR_A08	1p36.33	14.62	NM024848		Homo sapiens hypothetical protein FLJ13941 (FLJ13941), mRNA
10sBKR_A10	1 random	11.08	NM017891		Homo sapiens cDNA FLJ20584 fis, clone KAT09532
10sBKR_B10	11p15.5	3.66	NM173584		Homo sapiens hypothetical protein MGC45840 (MGC45840), mRNA
10sBKR_C04	6p21.33	1.14*	NM000434	22.94	Homo sapiens sialidase 1 (NEU1), mRNA
10sBKR_C07	20q13.33	23.92	NA		Homo sapiens expressed gene rerty
10sBKR_C09	22q12.2	16.80	NM030758		Homo sapiens oxysterol binding protein 2 (OSBP2), mRNA
10sBKR_C12	5p15.33	16.45	NA		Homo sapiens expressed gene rujy
10sBKR_D01	12q14.1	13.64	NM000785		Homo sapiens cytochrome P450, family 27, subfamily B, polypeptide 1, mRNA
10sBKR_D02	1p36.11	14.83	NM016124		Homo sapiens Rhesus blood group, D antigen (RHD), transcript variant 1, mRNA
10sBKR_D07	11q12.2	9.19	NM017870	2.58	Homo sapiens likely ortholog of rat GRP78-binding protein (GBP)
10sBKR_D10	1p36.32	15.03	NM005427	101.13	Homo sapiens tumour protein p73 (TP73), mRNA
10sBKR_E01	2q37.3	6.15	NM016510		Homo sapiens selenocysteine lyase (SCLY), mRNA
10sBKR_E04	17q21.2	9.19	NA		Homo sapiens expressed gene risiru
10sBKR_E05	3p22.2	2.17	NM033027		Homo sapiens AXIN1 up-regulated 1 (AXUD1), mRNA
10sBKR_E06	19p13.11	4.47	NM005919		Homo sapiens MADS box transcription enhancer factor 2
10sBKR_E07	20q13.32	4.72	NM001336	0.59*	Homo sapiens cathepsin Z (CTSZ), mRNA
10sBKR_E11†	19p13.3	12.91	NM004359	2.35	Homo sapiens cell division cycle 34 (CDC34), mRNA
			NM005317	1.739×10^6	Homo sapiens granzyme M (lymphocyte met-ase 1) (GZMM), mRNA
10sBKR_F01	7q22.1	9.13	NA		Homo sapiens expressed gene smerkar
10sBKR_F04	7p13	7.16	NM001220		Homo sapiens calcium/calmodulin-dependent protein kinase II beta, mRNA
10sBKR_F03	11q13.1	15.73	NM015080		Homo sapiens neurexin 2 (NRXN2), transcript variant alpha-1, mRNA
10sBKR_F05	6p21.31	7.78	NM003322		Homo sapiens tubby like protein 1 (TULP1), mRNA
10sBKR_F06	1 random	6.15	NA		Homo sapiens expressed gene zoyplaw
10sBKR_F09	17q21.33	13.09	NM002507	1144.10	Homo sapiens nerve growth factor receptor (NGFR), mRNA
10sBKR_F11	14q32.33	1.09*	NM001519		Homo sapiens BRF1 homolog, subunit of RNA polymerase III
10sBKR_F12	11p15.5	11.31	NM003957	0.89*	Homo sapiens serine/threonine kinase 29 (STK29), mRNA
10sBKR_G02	16p13.3	21.71	NM003834		Homo sapiens regulator of G-protein signalling 11 (RGS11), mRNA
10sBKR_G06	3p25.1	461.44	NM001998	4482.23	Homo sapiens fibulin 2 (FBLN2), mRNA
10sBKR_G07	Xp22.13	1.58	NA		Homo sapiens gene CA5B encoding carbonic anhydrase VB, mitochondrial
10sBKR_G09	19q13.43	7.84	NA		Homo sapiens gene muwaru encoding hypothetical protein MGC2752
10sBKR_G11	17q25.3	4.38	NM005993		Homo sapiens tubulin-specific chaperoned (TBCD), mRNA
10sBKR_G12	1q42.13	26.91	NM024554		Homo sapiens piggyBac transposable element derived 5 (PGBD5), mRNA
10sBKR_H05	19q13.42	4.44	NM013333		Homo sapiens epsin 1 (EPN1), mRNA

*Ratio of < 1.5. †The 10sBKR_E11 was mapped to a loci of two distinct genes. NA, not assigned.

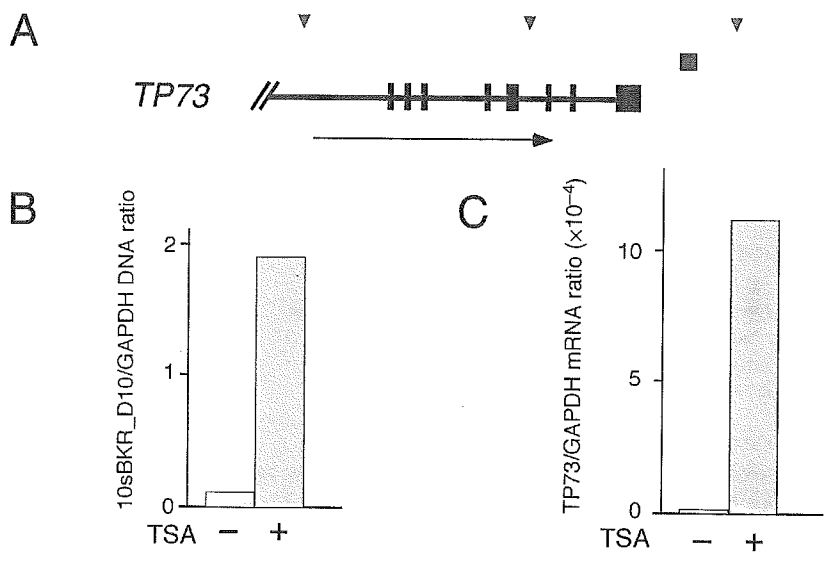

Figure 2 Identification of *TP73* as a target of HDAC activity. (A) one of the clones (10sBKR_D10; red rectangle) identified by DCS screening was mapped to chromosome 1p36.32, located ~1.2 kbp downstream of the last exon of *TP73*. Exons are denoted by black boxes, arrows indicate the direction of transcription, and green triangles depict distance markers of 5 kbp. (B) the amount of DNA corresponding to the 10sBKR_D10 sequence relative to the amount of that derived from *GAPDH* was measured by real-time PCR in the immunoprecipitates prepared with antibodies to acetylated histone H3 from MKN28 cells treated (+) or not (−) with TSA. (C) the amounts of *TP73* mRNAs relative to that of *GAPDH* mRNA in MKN28 cells treated or not with TSA were determined by real-time RT-PCR.

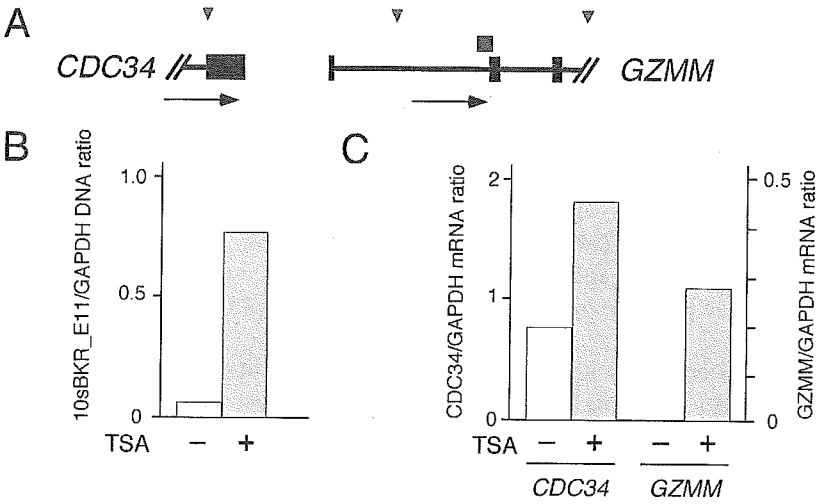

Figure 3 Identification of *CDC34* and *GZMM* as targets of HDAC activity. (A) one of the clones (10sBKR_E11; red rectangle) identified by DCS screening was mapped to chromosome 19p13.3, spanning the first intron and second exon of *GZMM* and located ~5 kbp downstream of the last exon of *CDC34*. The position of the 10sBKR_E11 in the genome is schematically shown as in Figure 2A. (B) The amount of DNA corresponding to the 10sBKR_E11 sequence relative to the amount of that derived from *GAPDH* was measured by real-time PCR. (C) the amounts of *CDC34* and *GZMM* mRNAs relative to that of *GAPDH* mRNA in MKN28 cells treated or not with TSA were determined by real-time RT-PCR.

on the *TP73* gene, and thereby regulates its transcriptional activity. Quantity of the genome fragment corresponding to the 10sBKR_D10 clone was measured by the real-time PCR method, revealing that its tester/driver ratio was 15.03 (Fig. 2B). Therefore, the extent of histone acetylation in this genome region in the tester cells was 15.03 times that in the driver cells. We also quantified the mRNA amount of *TP73* genes in both tester and driver cells by real-time reverse transcription (RT)-PCR method. As demonstrated in Fig. 2C, acetylation of the 10sBKR_D10 region was accompanied with a profound activation in the transcription level of *TP73*. These lines of evidence indicate that the *TP73* gene is epigenetically regulated by HDAC in a gastric cancer cell line.

Other targets of HDAC

One of our clones (10sBKR_E11) was mapped to a region which contains the first intron and the second exon of the *granzyme M* (*GZMM*) gene (GenBank accession number, NM_005317), and is also located ~5 kbp downstream of the last exon of *CDC34* (GenBank accession number, NM_004359) (Fig. 3A). Therefore, it was possible that histone acetylation of this region may affect the transcription of both genes. We first quantified the tester/driver ratio for the relative amount of the 10sBKR_E11 fragment in the acetylated histone H3 immunoprecipitates. As shown in Fig. 3B, histone at this region was more heavily acetylated in the tester cells compared to the driver cells.

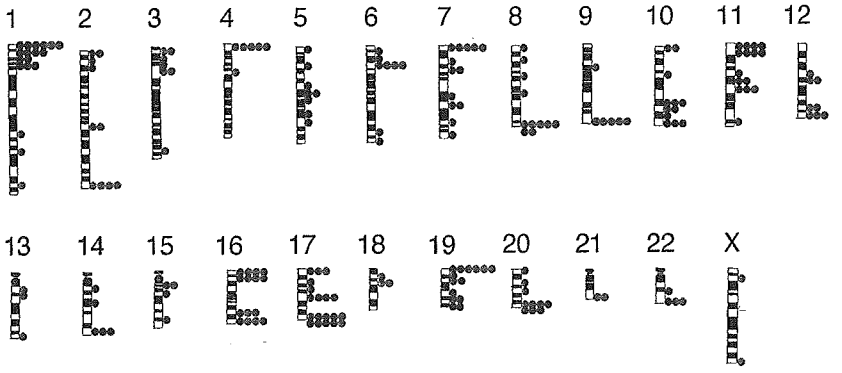

Figure 4 Chromosomal distribution of HDAC targets. The genome fragments (red dots) isolated by the DCS method were mapped to human chromosomes. The MKN28 cell line was established from a female and therefore does not contain the Y chromosome.

To examine how histone acetylation in this area affected the transcriptional activity of *CDC34* and *GZMM*, we measured the amounts of the corresponding mRNAs in both tester and driver cells by real-time RT-PCR. As demonstrated in Fig. 3C, histone acetylation up-regulated the expression of both *CDC34* and *GZMM*, although the extent of gene activation was greater for the latter than for the former. These data suggest that the histone acetylation status of a given genomic locus may regulate the transcription of distinct genes in a differential manner. Our data do not exclude the possibility, however, that histones in other regions of *CDC34* or *GZMM* were also acetylated in a TSA-dependent manner and that these regions possess an enhancer activity greater than that of the 10sBKR_E11 region.

CDC34 encodes a ubiquitin E2 ligase, and its activity is essential for G_1- to S-phase transition in cell cycle (Pagano *et al.* 1995). CDC34 catalyses ubiquitination of the inhibitors for cyclin-dependent kinases (CDKI) which are thereby subject to proteolysis. Therefore, it was interesting to find that *CDC34* gene was a target of HDAC in a cancer cell line.

We selected seven additional genes for quantification of the relative amounts of their mRNAs. Of the total of nine genes examined, seven genes were preferentially expressed in the TSA-treated cells compared with the non-treated cells (tester/driver ratio ≥ 1.5) (Table 1), consistent with the notion that histone acetylation results in the recruitment of transcription factors and consequent transcriptional activation.

Among the 136 clones that mapped within or close to known genes, only eight pairs were assigned to the same genes. Given the high fidelity of our DCS screening, these data suggest that HDAC complexes simultaneously act at hundreds of independent target histones within the same cell. To visualize directly the genome-wide HAP, we mapped to human chromosome figures our genomic clones whose chromosomal positions are known (Fig. 4). The HDAC targets were distributed widely throughout the human genome, although some 'hot spots' for deacetylation were apparent. Seven of our DCS clones were, for instance, mapped to the same 8q24.3 locus. Detailed mapping indicated that all these clones were located within a region spanning 2.5 Mbp. Therefore, it may be possible that regional alterations of chromatin structure lead to a coordinated transcriptional regulation of genes within the affected region.

Discussion

We have developed a rapid and highly reliable method for the selective isolation of genome fragments bound to histones whose level of acetylation differs between samples. Application of the DCS method to MKN28 cell line has readily revealed that many cell proliferation-associated genes are epigenetically regulated in cancer cells, including those for BMP7, TP73, GBP, AXUD1, CDC34, NGFR, RGS11 (see Table 1), JUNB, SIDEA, and MAFG (see Table S1).

Recently, similar genome-wide comparison methods have been developed by coupling chromatin immunoprecipitation (ChIP) with either comparative genomic hybridization (CGH) or analysis with a DNA microarray containing thousands of CpG islands or promoter fragments (Weinmann *et al.* 2002; Ballestar *et al.* 2003; Odom *et al.* 2004). However, the CGH analysis is not able to provide information on the precise genome sequences differentially immunoprecipitated, and the CpG array can only identify genome fragments that contain CpG islands. Interestingly, the majority of our clones identified by DCS do not satisfy the criteria of CpG islands (for instance, none of the clones corresponding to *TP73*, *CDC34-GZMM*, or *BMP7* was rich in the CpG sequence). Additionally, screening of whole promoter fragments is still hampered by the incomplete

human genome annotation and by its inability to investigate the enhancer regions. The emerging number of non-coding RNAs also makes it difficult to precisely map 'promoter' sequences in human genome. Therefore, for the identification of HAT-HDAC targets, our DCS method is likely to provide a non-biased means of genome-wide screening.

Although the study in this manuscript has revealed only the HDAC targets in a cancer cell line, the DCS method should be useful to directly identify HAT targets as well. For instance, a DCS comparison between chemotherapy-sensitive cancer cells and chemotherapy-resistant ones would enable to isolate genes whose associated histones are acetylated in a chemoresistance-dependent manner. In addition, DCS method can be applied to other non-malignant cells/tissues. We could indeed identify HDAC targets in cardiomyocytes (R.K., personal communication).

Furthermore, modification of our method may open up the possibility of a general ChIP-based subtraction strategy. For instance, DCS performed with antibodies to a given histone- or DNA-binding protein, rather than with antibodies to acetylated histone, should readily allow the isolation of target genomic fragments differentially recognized by such proteins.

Experimental procedures

Cell culture

MKN28 cells were obtained from the Japanese Collection of Research Bioresources (http://cellbank.nihs.go.jp/) and were maintained in RPMI 1640 medium (Invitrogen) supplemented with 10% foetal bovine serum. For preparation of the tester sample, cells were incubated for 24 h with 300 nM TSA (Wako, Tokyo, Japan). Satoh *et al.* (2002) have already demonstrated that, in MKN28 cells, histones of several genes become acetylated in a TSA-dependent manner.

The DCS method

Both formaldehyde treatment of cells and immunoprecipitation with antibodies to acetylated histone H3 were performed with the ChIP assay kit (#06-599; Upstate Biotechnology). Sonication of DNA was performed in one 10-s pulse to minimize the extent of DNA shearing (the resulting DNA fragments should migrate as a smear corresponding to a size of 10–20 kbp in gel electrophoresis). Immunoprecipitation was achieved with protein A-Sepharose beads (Sigma) suspended in TE (10 mM Tris-HCl, 7.4, and 0.1 mM EDTA) containing 0.2 mg/mL tRNA (Roche Biochemicals) and 0.5 mg/mL bovine serum albumin (New England Biolabs), instead of with the protein A beads supplied with the kit. DNA fragments were recovered from the immunoprecipitates and treated with RNase A to remove residual RNA. The DNA fragments were digested with *Rsa*I (New England Biolabs), and ligated to the TAG adaptor (5′-CCACCGCCATCCGAGCCTTTCTGCCCGGG-3′/3′-GAAAGACGGGCCC-5′). After PCR amplification with the TAG primer (5′-CCACCGCCATCCGAGCCTTTCTGC-3′), the tester DNA and the driver DNA were digested with *Xma*I and *Sma*I, respectively. Only the tester DNA (0.5 μg) was ligated to the first subtraction adaptor (5′-GTGAGGGTCGGATCT-GGCTGGCTC-3′/3′-CGACCGAGGGCC-5′). The adaptor-ligated tester DNA was then annealed with 40 μg of the driver DNA at 67 °C for 20–24 h before PCR amplification with the first subtraction primer (5′-GTGAGGGTCGGATCTGGCTGGCTC-3′). After digestion of single-stranded DNA with mung bean nuclease (New England Biolabs), the amplified products were subjected to digestion with XmaI followed by a second round of subtraction PCR with the second subtraction adaptor (5′-GTTAGCGGACACAGGGCGGGTCAC-3′/3′-GCCCAG-TGGGCC-5′) and second subtraction primer (5′-GTTAGCG-GACACAGGGCGGGTCAC-3′). The final products were digested with *Xma*I and ligated into pBlueScript (Stratagene) for nucleotide sequencing. The detailed protocol for the DCS method is available as a supplemental protocol online.

DNA quantification

Genome fragments immunoprecipitated by antibodies to acetylated histone H3 were subjected to PCR with a QuantiTect SYBR Green PCR Kit (Qiagen). The amplification protocol comprised incubations at 94 °C for 15 s, 62 °C for 30 s, and 72 °C for 60 s. Incorporation of the SYBR Green dye into PCR products was monitored in real time with an ABI PRISM 7700 sequence detection system (PE Applied Biosystems), thereby allowing determination of the threshold cycle (C_T) at which exponential amplification of PCR products begins. The C_T values for DNA molecules corresponding to the *GAPDH* gene and genome fragments of interest were used to calculate the abundance of the latter fragments relative to that of the former. The oligonucleotide primers for PCR were 5′-TCGGTGCGTGCCCAGTTGAACC-3′ and 5′-ATGCGGCTGACTGTCGAACAGGAG-3′ for *GAPDH*, 5′-ACCAGTCGCTGCTTTTAAATAAGG-3′ and 5′-GCTAGGAGCTTCCCCTACTAACAT-3′ for 10sBKR_D10, and 5′-CTGATGTGCGTTTTGAAGGACT-3′ and 5′-GAAACTTTTAGGCTGATACGTGTG-3′ for 10sBKR_E11.

mRNA quantification

Total RNA was prepared from the tester or driver cells with an RNeasy Mini column (Qiagen), treated with RNase-free DNase (Qiagen), and subjected to reverse transcription with PowerScript reverse transcriptase (BD Biosciences Clontech) with an oligo(dT) primer. Portions of the resulting cDNAs were subjected to PCR with a QuantiTect SYBR Green PCR Kit. The amplification protocol comprised incubations at 94 °C for 15 s, 65 °C for 30 s, and 72 °C for 60 s. The annealing temperature of PCR was changed to 60 °C for the cDNA of *CDC34* and 66 °C for that of *GZMM*. The oligonucleotide primers for PCR were 5′-AGAACATCATCCCTGCCTCTACT-3′ and 5′-

ATATTTGGCAGGTTTTTCTAGACG-3′ for *GAPDH*, 5′-GACGAGGACACGTACTACCTTCA-3′ and 5′-GTAGGTGACTCGGCCTCTGTAG-3′ for *TP73*, 5′-AAGATGTGGCACCCTAACATCTAC-3′ and 5′-AGGGAGATCACACTCAGGAGAAT-3′ for *CDC34*, and 5′-ATGTGTAACAACAGCCGCTTCT-3′ and 5′-CTTGAAGATGTCAGTGCAGACC-3′ for *GZMM*.

Acknowledgements

We thank Dr Kohei Miyazono for his helpful suggestions. This work was supported in part by a Grant-in-Aid for Research on the Second-Term Comprehensive 10-Year Strategy for Cancer Control from the Ministry of Health, Labor, and Welfare of Japan; a grant from Mitsubishi Pharma Research Foundation; a grant from Takeda Science Foundation; and a grant from Sankyo Foundation of Life Science.

Supplementary material

The following supplementary material is available from: http://www.blackwellpublishing.com/products/journals/suppmat/GTC/GTC804/GTC804sm.htm. **Appendix S1** The detailed protocol of the DCS method. **Table S1** All genome fragments isolated through the DCS screening.

References

Ballestar, E., Paz, M.F., Valle, L., *et al.* (2003) Methyl-CpG binding proteins identify novel sites of epigenetic inactivation in human cancer. *EMBO J.* **22**, 6335–6345.

Baylin, S.B. & Herman, J.G. (2000) DNA hypermethylation in tumorigenesis: epigenetics joins genetics. *Trends Genet.* **16**, 168–174.

Benard, J., Douc-Rasy, S. & Ahomadegbe, J.C. (2003) TP53 family members and human cancers. *Hum. Mutat.* **21**, 182–191.

Burgess-Beusse, B., Farrell, C., Gaszner, M., *et al.* (2002) The insulation of genes from external enhancers and silencing chromatin. *Proc. Natl. Acad. Sci. USA* **99** (Suppl. 4), 16433–16437.

Carrozza, M.J., Utley, R.T., Workman, J.L. & Cote, J. (2003) The diverse functions of histone acetyltransferase complexes. *Trends Genet.* **19**, 321–329.

Catley, L., Weisberg, E., Tai, Y.T., *et al.* (2003) NVP-LAQ824 is a potent novel histone deacetylase inhibitor with significant activity against multiple myeloma. *Blood* **102**, 2615–2622.

Gabrielli, B.G., Johnstone, R.W. & Saunders, N.A. (2002) Identifying molecular targets mediating the anticancer activity of histone deacetylase inhibitors: a work in progress. *Curr. Cancer Drug Targets* **2**, 337–353.

Gore, S.D., Weng, L.J., Zhai, S., *et al.* (2001) Impact of the putative differentiating agent sodium phenylbutyrate on myelodysplastic syndromes and acute myeloid leukemia. *Clin. Cancer Res.* **7**, 2330–2339.

Grignani, F., De Matteis, S., Nervi, C., *et al.* (1998) Fusion proteins of the retinoic acid receptor-alpha recruit histone deacetylase in promyelocytic leukaemia. *Nature* **391**, 815–818.

Kaghad, M., Bonnet, H., Yang, A., *et al.* (1997) Monoallelically expressed gene related to p53 at 1p36, a region frequently deleted in neuroblastoma and other human cancers. *Cell* **90**, 809–819.

Kent, W.J. (2002) BLAT—the BLAST-like alignment tool. *Genome Res.* **12**, 656–664.

Kouzarides, T. (1999) Histone acetylases and deacetylases in cell proliferation. *Curr. Opin. Genet. Dev.* **9**, 40–48.

van Leeuwen, F. & Gottschling, D.E. (2002) Genome-wide histone modifications: gaining specificity by preventing promiscuity. *Curr. Opin. Cell Biol.* **14**, 756–762.

Lin, R.J., Nagy, L., Inoue, S., Shao, W., Miller, W.H. Jr & Evans, R.M. (1998) Role of the histone deacetylase complex in acute promyelocytic leukaemia. *Nature* **391**, 811–814.

Odom, D.T., Zizlsperger, N., Gordon, D.B., *et al.* (2004) Control of pancreas and liver gene expression by HNF transcription factors. *Science* **303**, 1378–1381.

Pagano, M., Tam, S.W., Theodoras, A.M., *et al.* (1995) Role of the ubiquitin-proteasome pathway in regulating abundance of the cyclin-dependent kinase inhibitor p27. *Science* **269**, 682–685.

Satoh, A., Toyota, M., Itoh, F., *et al.* (2002) DNA methylation and histone deacetylation associated with silencing DAP kinase gene expression in colorectal and gastric cancers. *Br. J. Cancer* **86**, 1817–1823.

Toyota, M., Ho, C., Ahuja, N., *et al.* (1999) Identification of differentially methylated sequences in colorectal cancer by methylated CpG island amplification. *Cancer Res.* **59**, 2307–2312.

Verdin, E., Dequiedt, F. & Kasler, H.G. (2003) Class II histone deacetylases: versatile regulators. *Trends Genet.* **19**, 286–293.

Waterborg, J.H. (2002) Dynamics of histone acetylation in vivo. A function for acetylation turnover? *Biochem. Cell Biol.* **80**, 363–378.

Weinmann, A.S., Yan, P.S., Oberley, M.J., Huang, T.H. & Farnham, P.J. (2002) Isolating human transcription factor targets by coupling chromatin immunoprecipitation and CpG island microarray analysis. *Genes Dev.* **16**, 235–244.

Yasui, W., Oue, N., Ono, S., Mitani, Y., Ito, R. & Nakayama, H. (2003) Histone acetylation and gastrointestinal carcinogenesis. *Ann. NY. Acad. Sci.* **983**, 220–231.

Received: 21 August 2004
Accepted: 16 September 2004

Available online at www.sciencedirect.com
SCIENCE DIRECT®
Biochemical and Biophysical Research Communications 320 (2004) 1328–1336
BBRC
www.elsevier.com/locate/ybbrc

Cardiac function-related gene expression profiles in human atrial myocytes ☆

Ruri Ohki-Kaneda [a,b], Jun Ohashi [c], Keiji Yamamoto [b], Shuichi Ueno [a,b], Jun Ota [a,d], Young Lim Choi [a], Koji Koinuma [a], Yoshihiro Yamashita [a], Yoshio Misawa [e], Katsuo Fuse [e], Uichi Ikeda [b], Kazuyuki Shimada [b], Hiroyuki Mano [a,d,*]

[a] *Division of Functional Genomics, Jichi Medical School, 3311-1 Yakushiji, Kawachigun, Tochigi 329-0498, Japan*
[b] *Division of Cardiology, Jichi Medical School, 3311-1 Yakushiji, Kawachigun, Tochigi 329-0498, Japan*
[c] *Department of Human Genetics, Graduate School of Medicine, University of Tokyo, Tokyo 113-0033, Japan*
[d] *CREST, JST, Saitama 332-0012, Japan*
[e] *Division of Cardiovascular Surgery, Jichi Medical School, 3311-1 Yakushiji, Kawachigun, Tochigi 329-0498, Japan*

Received 6 May 2004
Available online 2 July 2004

Abstract

To obtain insights into the molecular pathogenesis of heart failure in humans, we have analyzed the expression profiles of >12,000 genes in a total of 17 human specimens of right atrial myocytes. From this large data set, we here tried to identify gene clusters, expression level of which is correlated precisely with clinical parameter values of cardiac function. We could reveal that cardiac myocytes with normal sinus rhythm were clearly differentiated, in the point of view of gene expression, from those with atrial fibrillation. Further, an expression profile-based prediction of arrhythmia by a newly developed "weighted-distance method" could efficiently diagnose our samples. We could even construct calculation formulae for the values of left ventricular ejection fraction based on the expression level of selected genes. To our best knowledge, this is the first report to indicate that pumping ability of heart can be predicted by any measures of atrium.

Keywords: DNA microarray; Heart failure; Ejection fraction; Correspondence analysis

The pumping failure of heart, or heart failure, is induced by a variety of pathological conditions, such as ischemic heart diseases, arrhythmias, and sustained pressure- or volume-overload onto heart [1]. It is still highly difficult to restore the contractile ability of cardiac myocytes in once failed heart, and, therefore, heart failure is still one of the main causes for human death [2]. Unfortunately, little is still understood for the molecular mechanisms underlying why and how heart failure is developed and becomes irreversible.

Although cardiac myocytes in culture may be a useful means to analyze the intracellular signaling pathways responsible for hypertrophic changes in heart, such in vitro systems cannot efficiently simulate the long-term changes of myocytes found in failed heart. To decipher the molecular pathology of heart failure, therefore, it would be indispensable to directly investigate the human specimens of failed heart or to analyze myocytes in model animals for heart failure.

☆ *Abbreviations:* Af, atrial fibrillation; EF, ejection fraction; TR, tricuspid valve regurgitation; MR, mitral valve regurgitation; LAD, left atrial diameter; RT-PCR, real-time reverse transcription-polymerase chain reaction; GAPDH, glyceraldehyde-3-phosphate dehydrogenase.

* Corresponding author. Fax: +81-285-44-7322.
E-mail address: hmano@jichi.ac.jp (H. Mano).

0006-291X/$ - see front matter © 2004 Elsevier Inc. All rights reserved.
doi:10.1016/j.bbrc.2004.06.090

Toward this goal, we have recently collected human specimens of right atrial myocytes from patients with various heart disorders, and obtained the expression profiles of >12,000 genes in the samples by using high-density oligonucleotide microarrays (R.O. et al., submitted). Since the patients in the analysis could be classified into two major groups, i.e., individuals with either normal sinus rhythm or an arrhythmia, chronic atrial fibrillation (Af), we first tried to identify gene sets, expression of which were associated with the presence/absence of chronic Af in vivo. A total of 33 genes were shown to be induced (>1.5-fold) in Af samples compared to those with normal sinus rhythm, while 63 genes were to be suppressed (<0.5-fold) in the Af-ones.

However, such analyses did not fully address a fundamental question as to whether atrial myocytes with Af have a distinct gene expression profile, or "molecular signature" [3], to those with normal sinus rhythm. In other words, with regard to gene expression profiles, are the myocytes with Af distinct from those with normal rhythm?

In this paper, by applying sophisticated statistical methods, we have tried to address these issues. Furthermore, we here tested whether it was possible to identify gene sets, expression level of which was precisely correlated with detailed clinical parameter values of cardiac function. The results were highly successful, and we could even construct "prediction formulae for the values of left ventricular ejection fraction (EF)" based on the expression level of selected genes. To our best knowledge, this is the first report to prove that pumping ability of heart can be predicted by any measures of atrium.

Materials and methods

Microarray analysis. Detailed information on the patients registered for this study and on the microarray experiments will be reported elsewhere (R.O. et al., submitted). Left ventricular EF values in all patients was calculated by dividing the stroke volume (end-diastolic volume minus end-systolic volume) by the end-diastolic volume (both obtained angiographically). From the patients who underwent cardiac surgery in Jichi Medical School, right atrial appendages were obtained with written informed consent. Total RNA was extracted from the specimens with the use of RNAzol B (Tel-Test, Friendswood, TX), and a portion (20 μg) of the RNA was converted to double-stranded cDNA by the SuperScript Choice System (Life Technologies, Gaithersburg, MD). Biotin-labeled cRNA was prepared from the resulting cDNA with the use of ENZO BioArray RNA labeling kit (ENZO Diagnostics, Farmingdale, NY), and hybridized with the GeneChip Human U95Av2 array (Affymetrix, Santa Clara, CA) harboring the oligonucleotides corresponding to >12,000 human genes. Detection of the hybridized cRNAs was performed with the GeneChip instrument system according to the manufacturer's protocol. The fluorescence intensity of each gene was normalized relative to the median fluorescence value for all genes in each array hybridization.

Statistical analysis. In the comparison of normal sinus rhythm- vs Af-specimens, t statistic and the effect size (difference in the mean of expression levels between the two classes) [4] were calculated for each gene. When the gene showed $|t| > 4.073$ (corresponding to a significance level of 0.001 in t test with 15 degrees of freedom) and |effect size| > 0.5 arbitrary units (U), the difference in expression level between the two classes was regarded as statistically significant. Correspondence analysis [5] was carried out for all genes showing the significant difference by using the ViSta computer software (http://www.visualstats.org/). Each sample was plotted in three dimensions based on the coordinates of the three major dimensions from correspondence analysis.

To examine whether these informative genes could predict the class of the present samples, we have here developed a novel class prediction means, "weighted-distance method," with the points of dimensions obtained from correspondence analysis. There were a total of 17 samples: 10 specimens with sinus rhythm and 7 with Af arrhythmia. A correspondence analysis was conducted once for all 17 samples, and the class prediction was performed for each sample (say sample X) under the condition that the classes of only remaining 16 samples were known. The weighted distance from sample X to sample Y ($Y \neq X$) is defined as $D = \sqrt{\sum_{i=1}^{k} [v_i (d_i^X - d_i^Y)^2]}$, where k is the number of dimensions to be considered, v_i indicates the contribution of the ith dimension, and d_i^X and d_i^Y represent points of the ith dimension for sample X and sample Y, respectively. Because v_1 exceeded 70% in our analysis (i.e., the cumulative contribution to the 1st dimension was very large), k was set to be 1 in this study (i.e., $D = \sqrt{v_1 (d_1^X - d_1^Y)^2}$). In general, k should be determined by the cumulative contribution to the kth dimension. Let D_S and D_A be the averages of weighted distance (D) from sample X to sinus rhythm samples and from sample X to the Af samples, respectively. When $D_S/(D_S + D_A)$ was below a threshold value, T, the sample X was assigned a "sinus rhythm" class, and when $D_A/(D_S + D_A)$ was below T, the sample X was assigned an "Af" one. In this study, T was set to be 0.4.

Correlation to the clinical grade of tricuspid valve regurgitation (TR) or mitral valve regurgitation (MR) was calculated for the expression level of each gene by a paired Spearman's rank test, and was considered as statistically significant when $P < 0.001$. Similarly, Pearson's correlation coefficient (r) for EF (in percents) or left atrial diameter (LAD) (in millimeters) was examined for the expression level of each gene.

For each of the EF-linked genes identified above, we conducted the simple regression analysis to generate an EF-calculation formula "$y = Ax + B$," where y is EF (%) and x is the expression level (U) of each gene.

All raw microarray data as well as the details of the genes shown in the figures are available as supplementary information at the web site of *Biochem. Biophys. Res. Commun.*

Real-time reverse transcription-polymerase chain reaction (RT-PCR). Portions of nonamplified cDNA were subjected to PCR with a QuantiTect SYBR Green PCR Kit (Qiagen, Valencia, CA). The amplification protocol comprised incubations at 94 °C for 15 s, 60 °C for 30 s, and 72 °C for 60 s. Incorporation of the SYBR Green dye into PCR products was monitored in real time with an ABI PRISM 7700 sequence detection system (PE Applied Biosystems, Foster City, CA), thereby allowing determination of the threshold cycle (C_T) at which exponential amplification of PCR products begins. The C_T values for cDNAs corresponding to the glyceraldehyde-3-phosphate dehydrogenase (GAPDH) and *Calpactin I* genes were used to calculate the abundance of *Calpactin I* mRNA relative to that of *GAPDH* mRNA. The oligonucleotide primers for PCR were 5′-GTCAGTGGTG GACCTGACCT-3′ and 5′-TGAGCTTGACAAAGTGG TCG-3′ for *GAPDH* cDNA and 5′-TCTGGCTGTGGACAAAATAATG-3′ and 5′-TTTCCCTTCTGCTTCATGTGTA-3′ for *Calpactin I* cDNA.

Results

Isolation of genes linked to arrhythmia

Among the 17 samples analyzed, 7 were obtained from the patients with chronic, persistent Af and the rest

Table 1
Characteristics of the study subjects

Patient ID	Age	Sex	Disease	MR grade	TR grade	LAD (mm)	Rhythm	EF (%)
1	44	M	AR	0	1	39.7	Sinus	49
2	70	F	MR	3	1	50.1	Sinus	48
3	75	M	IHD	1	1	39	Sinus	61
4	65	M	AS	1	0	45.1	Sinus	71
5	60	M	AS	2	0	39.7	Sinus	33
6	51	F	MS	0	3	71	Af	78
7	55	M	MR	4	2	69.4	Af	55
9	64	M	MR	4	2	77	Af	68
10	74	F	MSR, ASR	3	2	61.1	Af	66
11	75	M	ASR, MR	3	2	59	Af	37
12	64	F	MR	3	3.5	48	Sinus	65
13	64	F	MR, AR	4	3.5	42	Sinus	80
14	14	M	ASD	0	2	32.1	Sinus	67
15	59	F	MS, AR	2	4	76.7	Af	70
16	69	F	MSR, AR	3	4	54	Af	57.5
17	63	M	AR, MR	2	3	52	Sinus	50
18	37	F	ASD	2	0	35	Sinus	60

M, male; F, female; AR, aortic regurgitation; IHD, ischemic heart disease; AS, aortic stenosis; MS, mitral stenosis; MSR, mitral stenosis/regurgitation; ASR, aortic stenosis/regurgitation; ASD, atrial septal defect.

10 were from those with normal sinus rhythm (Table 1). Identification of any genes constantly activated or inactivated in Af samples would shed new light on the pathophysiology of this most prevalent arrhythmia [6]. First, identified were the genes whose expression levels were statistically different (Student's t test, $P<0.001$) between the two classes, i.e., normal sinus rhythm and Af. However, expression levels of many such genes were very low throughout the samples, making the reliability of "arrhythmia-dependence" obscure. Therefore, we further applied another "selection window" that the effect size should be >0.5 U between the two classes, leading to the identification of 11 arrhythmia-dependent genes, expression profile of which should most effectively contrast Af status from normal sinus rhythm.

A dendrogram or "gene tree" is demonstrated in Fig. 1A for these genes including those encoding for sarcoglycan ε (SGCE; GenBank Accession No. NM_003919), zinc finger protein 103 (ZFP103; NM_005667), and hepatic leukemia factor (HLF; NM_002126). Here in the tree, genes with similar expression pattern across the samples were placed near each other. HLF is a helix–loop–helix type transcriptional factor that functions to protect cells from apoptosis [7]. Decreased expression of *HLF* in the myocytes with Af arrhythmia may reflect the apoptotic change found in atrial remodeling.

Expression profile-based prediction of Af

In the point of view of gene expression profile, are the myocytes with Af arrhythmia different from those with normal sinus rhythm, and, if so, how different? We tried to address this issue by the correspondence analysis to extract three major dimensions from the expression patterns of the 11 arrhythmia-dependent genes. By the calculated coordinates for each sample in these dimensions, the patient samples were projected into the virtual space with the three dimensions. Surprisingly, as shown in Fig. 1B, all samples with Af were clustered in an area clearly far from that for the samples with sinus rhythm. It is, therefore, likely that all Af samples have a common "gene expression signature" which is distinct from that for sinus rhythm samples.

The clear separation of Af and sinus rhythm specimens in Fig. 1B also indicates a possibility of an expression profile-based prediction for Af. As demonstrated in Fig. 1B, class-separation was most prominent in the 1st dimension. Indeed, the contribution ratio of each dimension calculated by the correspondence analysis was 72.74%, 9.5%, and 6.29% for the 1st, 2nd, and 3rd dimensions, respectively. Therefore, we tried to conduct the class prediction (i.e., Af or sinus rhythm) for each sample by using the coordinates for the 1st dimension. The relative distance of a given sample to the Af or sinus rhythm group (excluding the sample for prediction) was calculated, and the sample was assigned a class when the relative distance to the class was $\leqslant 0.4$. As shown in Table 2, the class prediction based on the correspondence analysis with the 11 genes in Fig. 1A was successful for all cases.

To accurately measure the prediction power of our weighted distance method, we conducted a cross-validation trial (i.e., "drop-one-out" format) for the diagnosis of normal sinus rhythm or chronic Af class. To predict the class of sample X, "arrhythmia-associated genes" were extracted from the comparison of remaining 16 samples according to the criteria used in Fig. 1A ($P<0.001$ in Student's t test, and |effect size| > 0.5 U). Correspondence analysis was carried out for the expression profiles of the arrhythmia-associated genes, and